Title Page

Title:

Intestinal adaptations increase basolateral intestinal glucose uptake and glycolysis in a mouse model of Cystic Fibrosis

Authors:

Alexander F Lesser
Department of Pathology, Case Western Reserve University, Cleveland OH 44106, USA
Department of Genetics and Genome Sciences, Case Western Reserve University, Cleveland OH 44106, USA

Aura Perez
Department of Genetics and Genome Sciences, Case Western Reserve University, Cleveland OH 44106, USA

Chunying Wu, PhD
Department of Radiology, Case Western Reserve University, Cleveland OH 44106, USA

Shuyu Hao
Department of Genetics and Genome Sciences, Case Western Reserve University, Cleveland OH 44106, USA

Bernadette Erokwu, DVM
Department of Radiology, Case Western Reserve University, Cleveland OH 44106, USA

Derek Host
Department of Nutrition, Case Western Reserve University, Cleveland OH 44106, USA
Department of Genetics and Genome Sciences, Case Western Reserve University, Cleveland OH 44106, USA

Anjum Jafri
Department of Genetics and Genome Sciences, Case Western Reserve University, Cleveland OH 44106, USA

Elisha Barbato
Department of Genetics and Genome Sciences, Case Western Reserve University, Cleveland OH 44106, USA

Lauren Yeh, BS
Department of Genetics and Genome Sciences, Case Western Reserve University, Cleveland OH 44106, USA

Jean Eastman
Department of Genetics and Genome Sciences, Case Western Reserve University, Cleveland OH 44106, USA

Senthilkumar Sankararaman
Department of Pediatric Gastroenterology, Hepatology, and Nutrition, Cleveland Clinic, Cleveland OH 44195 USA

Chris A Flask, PhD
Department of Radiology, Case Western Reserve University, Cleveland OH 44106, USA
Department of Biomedical Engineering, Case Western Reserve University, Cleveland OH 44106, USA
Department of Pediatrics, Case Western Reserve University, Cleveland OH 44106, USA

Mitchell L Drumm (corresponding author)
Department of Genetics and Genome Sciences, Case Western Reserve University,
824 BRB
2109 Adelbert Rd
Cleveland OH 44106, USA
mitchell.drumm@case.edu,
216-368-6893

Intestinal adaptations increase basolateral intestinal glucose uptake and glycolysis in a mouse model of Cystic Fibrosis

ABSTRACT

The gastrointestinal manifestations of Cystic Fibrosis (CF) are a continued source of morbidity and mechanistic uncertainty despite recent advances in CF care. We sought to characterize intestinal glucose demand in a mouse model of CF to better understand CF intestinal disease. We assessed *in vivo* systemic glucose uptake from circulation, including intestinal glucose demand, using ^{18}F-Fluorodeoxyglucose Positron Emission Tomography (PET) imaging studies in wildtype (WT) and CF mice. RNA-Sequencing studies with complementary assessments of protein expression and functional metabolism were performed to identify the responsible glucose transporter and relevant metabolic pathways. Lastly, morphologic and histologic differences between the CF and WT small intestine were investigated. Increased glucose uptake from circulation to CF intestine was detected with the most prominent increases seen in CF jejunum and ileum. Increased mRNA and protein expression of GLUT1 was evident in whole intestinal tissue and isolated crypts suggesting GLUT1 is responsible for mediating the increased glucose uptake from the blood supply. We found transcriptional and functional enrichment of glycolysis in the CF jejunum and ileum. Proliferative intestinal adaptations, including increased intestinal length and weight, in addition to increased villi length and crypt depth, were observed in CF mice. The increased intestinal glucose uptake from circulation and increased glycolysis, in combination with the morphologic and histologic changes in the CF intestine,

are suggestive of a proliferative adaptive response and increased intestinal glucose demand in CF. This work may yield novel markers of CF disease status and new therapeutic approaches.

NEW AND NOTEWORTHY

We found transcriptional, protein level, and functional evidence of increased intestinal glucose uptake from circulation and increased glycolysis in a Cystic Fibrosis mouse model. These findings in the context of hyperplastic morphologic and histologic changes in the Cystic Fibrosis intestine are indicative of an adaptive response. Our work elucidates new mechanisms of intestinal disease in Cystic Fibrosis and identifies altered intestinal glucose uptake and glycolysis as potential markers of disease status and gastrointestinal cancer risk.

Keywords: Cystic Fibrosis, Intestine, Glucose Metabolism, Glucose Uptake, Intestinal Adaptation

INTRODUCTION

The intestinal manifestations of Cystic Fibrosis (CF) continue to be a source of morbidity despite major advances in CF therapies over the past several years (1). CF intestinal disease may include obstruction at birth or throughout the lifespan, dysmotility, constipation, small intestinal bacterial overgrowth, and abdominal pain and discomfort (2). People with CF also have a five to ten-fold increased risk of developing gastrointestinal cancers earlier in life, the reason for which remains largely unknown (3–

5). The mechanisms underlying the intestinal manifestations of CF are not fully understood. Impaired chloride and bicarbonate ion transport due to absent or dysfunctional CFTR results in dehydrated, viscous mucus that coats the intestinal lumen and alters pH. These changes are thought to create an environment that hinders digestive enzymatic and immune function to promote dysbiosis, dysmotility, and obstruction (2, 6, 7). The other major organs of digestion, including the pancreas and hepatobiliary system, are also affected in CF, which can result in a variety of symptoms mainly related to fat malabsorption, in addition to various hepatic and biliary pathologies (2, 7).

Most of what is known about the CF intestines has been garnered from studies on the luminal function pertaining to digestion, absorption, mucus accumulation, and bacterial dysbiosis, but little has been described regarding the serosal side. In the process of evaluating systemic carbohydrate utilization in CF mice, we identified the intestine as a key site of increased glucose uptake from circulation in CF. Consequently, we employed a series of complementary *in vivo* and *ex vivo*, transcriptional and functional approaches to characterize intestinal glucose demand and metabolism in a mouse model of CF to gain new insights into mechanisms of intestinal disease.

We show elevated GLUT1 (*Slc2a1*) expression in both CF intestinal tissue and isolated crypts, suggesting GLUT1 is responsible for the increased intestinal glucose uptake from the circulation in CF mice. We also identified concomitant increases in glycolysis, in addition to evidence of increased cell proliferation in the CF intestine. Taken together, these results are indicative of an increased intestinal glucose demand in CF to maintain intestinal homeostasis. This work offers a novel approach to

understanding CF intestinal disease. Our findings emphasize a continued need to investigate how the interplay of numerous digestive and absorptive defects in CF contribute to disease pathogenesis to develop more effective therapies for the gastrointestinal manifestations of CF.

MATERIALS AND METHODS

Mouse model

All experiments were performed using age and sex matched, non-littermate wildtype (WT) and the previously established Cystic Fibrosis (CF) (G542X/G542X) mice on the C57Bl6/J background (8). Male and female mice, approximately 6-12 weeks of age, were used for all experiments unless otherwise indicated. All mice had unrestricted access to D12451i diet (Research Diets, 45 kcal % fat) with acidified water. Mice were housed in standard, ventilated polysulfone microisolator cages with corncob bedding, nestlets, and shelter and maintained on a 12hr light/12hr dark cycle schedule with an average ambient temperature of 22ºC. All interventions and sample collection were performed during the light cycle. All animal use and procedures were approved by Case Western Reserve University's Institutional Animal Care and Use Committee (IACUC).

In vivo ^{18}F-FDG Positron Emission Tomography (PET)/Magnetic Resonance Imaging (MRI) studies

Mice were fasted for 4 hours prior to imaging studies and moved to cages with Alpha-Dri™ bedding with free access to water. ^{18}F-Fluorodeoxyglucose (~200µC, 7.4MBq ^{18}F-FDG per mouse) was injected through the tail vein. The mice were then

anesthetized with isoflurane and positioned within a Bruker Biospec 0.4T MRI scanner (Bruker Corp., Billerica, MA, USA) employing a Cubresa NuPET PET insert (Cubresa Inc., Winnipeg Mannitoba, Canada) to acquire the PET signals as well as a PET compatible radiofrequency volume MRI coil (ID = 35 mm) to acquire the MRI signals. The PET and MRI data were acquired simultaneously. A 90-minute dynamic PET scan was used to acquire the PET images, while a coronal 3D True FISP (True Fast Imaging with Steady-state Free Precession) acquisition was used to generate the anatomic MRI images (FOV = 60 x 30 x 30mm, matrix size = 256 x 128 x 128, TR/TE = 4.0/2.0 ms, flip angle = 30 degrees, 5 signal averages, scan time = 6 minutes). Body temperature and respiration of the anesthetized mice were monitored and maintained during the PET-MRI scans.

Ex vivo ^{18}F-FDG biodistribution studies

Following the ^{18}F-FDG *in vivo* imaging studies, sections of duodenum, jejunum, ileum, and central colon exclusive of the cecum were collected and weighed with and without intestinal contents. Radioactivity of the respective intestinal pieces was assayed by gamma counter (Lablogic, Hidex-AMG). Samples then air-dried overnight followed by 24hrs at 60°C for determination of the dry weight.

RNA isolation

The small intestine was extracted in its entirety from stomach to cecum and flushed with cold phosphate buffered saline (PBS). Three-inch long intestinal segments were collected from the beginning, middle and end of the small intestine to correspond

with duodenum, jejunum, and ileum respectively and frozen immediately in liquid nitrogen. The jejunum section was divided in half lengthwise prior to freezing, using one section for whole tissue RNA and the other for crypt isolation and subsequent RNA extraction. RNA was isolated using Rneasy mini kit (Qiagen), concentration and quality checked with the Nanodrop (ThermoScientific).

Intestinal crypt isolation

The respective intestinal sections were flushed with cold PBS. Sections were then cut longitudinally and villi removed with gentle scraping. Intestinal sections were then cut into small pieces and rocked in PBS-EDTA (Phosphate-buffered saline-Ethylenediaminetetraacetic acid) (2mM, pH 8) at max speed using the Boekel Ocelot Shaker (Model 260300F, Fisher Scientific) for 30 minutes for dissociation at room temperature. Samples were then vortexed for approximately 10 seconds, allowed to settle, and the supernatant removed and collected. Fresh PBS was added and the process repeated for a total of 4 times to obtain 4 total fractions. The 3rd and 4th fractions were used and centrifuged at 200 RCF for 10 minutes at 4°C and supernatant removed.

Protein isolation and western blot

Isolated crypts and PBS-washed whole intestinal tissue samples were respectively lysed and homogenized with RIPA (radio-immunoprecipitation assay) buffer (Thermo Fisher, #89901) containing protease inhibitors (Complete, EDTA-free Protease Inhibitor Cocktail tablets, Roche). Samples were incubated either on ice for 30 minutes or for 2 hours at 4°C for crypts and whole tissue lysates respectively. Protein was

quantified by BCA (bicinchoninic acid) assay (BioRad). Samples were prepared in 4x Laemmli sample buffer (BioRad) and either incubated at room temperature for 30 minutes for GLUT1 blots or at 95°C for 5 minutes for Hexokinase2 (HK2) blots. Samples were loaded into a precast 12% polyacrylamide gel or 8-16% polyacrylamide gel (BioRad) for GLUT1 and HK2 blots respectively. Protein was transferred to polyvinylidene fluoride microporous membranes (Millipore) using the Trans-Blot Turbo Blotting System (BioRad). Membranes were blocked in 5% nonfat milk prepared in PBS with 0.01% Tween-20 for 1 hour at room temperature and then incubated overnight with anti-GLUT1 antibody (ab115730, 1:10,000), anti-Hexokinase II antibody (ab209847, 1:1000), or anti-beta-Actin antibody (Cell Signaling, Cat#4970, 1:1000). Blots were incubated at 4ºC overnight in 5% of non-fat dry milk in 1xPBS-T (0.1% Tween 20 in 1x PBS) with gentle shaking using the Labnet Shaker 35. Mouse anti-rabbit IgG antibody, HRP conjugate (Millipore, AP188P) was used as the secondary antibody. Immunoblot signal was detected using a ChemDoc imaging system (BioRad).

***Ex vivo assessments of* extracellular acidification rate**

Tissue extracellular acidification rate for intestinal tissue was assessed using a modified protocol from Fan *et al*. (2022) (9). Small intestinal segments were washed in ice cold PBS and the contents were gently removed. A 2mm biopsy puncher (Qiagen) was used to make 5-7 equally sized tissue pieces per intestinal section. Each intestinal punch was added into a single well of an Islet XF24 microcapture plate and held into place with an islet screen (Agilent). Wash media (Gibco 11885-084, supplemented with 25mM HEPES (4-(2-hydroxyethyl)-1-piperazineethanesulfonic acid) and additional

glucose to reach 25mM total) was added to each well. Then, tissue pieces were washed with wash media followed by assay media (Agilent 103575-100, supplemented with 17.5mM glucose, 1mM pyruvate, 4mM glutamine). Next, assay media was added to each well and the plate incubated at 37°C for 45 minutes. Following the incubation, media was replaced with fresh assay media. The Seahorse XFe24 Analyzer and corresponding XFe24 sensor cartridges (Agilent) were used to measure the baseline oxygen consumption rate (OCR) and extracellular acidification rate (ECAR). Ten measurement cycles were obtained. The XFe24 Analyzer measurement parameters were set to the machine standard of 3 minutes for “Mix,” 2 minutes for “Wait,” and 3 minutes for “Measure” for each measurement cycle. All steps prior to the incubation were performed on ice.

Lactate quantification

For each intestinal section, 4-5 equally sized 2mm tissue punches were obtained and prepared in the exact same manner as for the *ex vivo* studies of extracellular acidification rate. Following 45 minutes of incubation, media was collected. Lactate levels were measured using RayBioTech L-Lactate assay (MA-LAC-1). Data are presented as average fold change of replicates relative to WT controls.

Histology

Small intestines were excised from stomach to cecum and flushed with cold PBS. Samples for intestinal cross sections were then cut into approximately 1 cm sections from each intestinal region. For layer quantification studies, the intestine was divided

into 5 equal consecutive sections and each opened longitudinally. Swiss rolls for each section were prepared using a modified protocol from Williams *et al.* (10). Intestinal samples were fixed in a 10% neutral buffered formalin solution for 24 hours. Samples were then processed and embedded in paraffin using standard histological procedures. The tissue blocks were then sectioned into 5-micron slices and mounted on glass slides. Hematoxylin and eosin staining was performed following a standard protocol for tissue analysis. Images were taken using an Olympus BX43 microscope with LC35 USB camera and are displayed at 4X or 10X magnification. For quantification of the intestinal layer thickness, slides were scanned with a Hamamatsu Nanozoomer S60 at 40X.

Data Analyses

^{18}F-FDG PET/MR image analyses and quantification

PET and MR image registration and quantitative image analysis of ^{18}F-FDG uptake in different organs was performed using VivoQuant software. Regions of interest (ROI) were extrapolated from the reconstructed μPET image frames and standard uptake value (SUV) was quantified in a specific region based on the PET and MR co-registered images. The radioactivity data were decay-corrected and normalized to the body weight and the amount of ^{18}F-FDG injected. Radioactivity concentration in the respective organs is expressed in terms of SUV. The time activity curve (TAC) for each organ was obtained.

Biodistribution studies

Tissue activity was decay-corrected to the euthanasia time and was divided by the injected activity in order to determine the percent of injected dose (%ID). This was, in turn, divided by the tissue mass to determine the activity expressed as the percent of the injected dose per gram of tissue (%ID/g) using the wet weight, in accordance with the field standard analytic approach for biodistribution studies. Data were also normalized to dry weight. Decay-corrected activity normalized to dry weight was also calculated (MBq/g dry weight).

RNA-sequencing studies

RNA-seq libraries were generated using TruSeq stranded Total RNA Ribo-Zero mouse gold kit (Illumina, San Diego, CA) and the quality of resulting libraries was assessed using Agilent 2100 Bioanalyzer (Agilent Technologies, Inc., Santa Clara, CA). Ileum (WT n=4, CF n=5) sequencing was carried out using an Illumina HiSeq 2500 Rapid Run flow cell – 2x100bp run. Duodenum (WT n=9, CF n=9), jejunum (WT n=8, CF n=9) and jejunum crypts (WT n=8, CF n=9) sequencing was carried out using an Illumina NextSeq 550 HO flowcell – 2x75bp run. Reads were trimmed and filtered using Trimmomatic (v 0.39), then aligned to UCSC (University of California Santa Cruz) mouse genome mm10 using Bowtie2 and Tophat (2.1.1). Assembly of transcriptomes and quantification was performed with Cufflinks (2.1.1). Expression levels are expressed as fragments per kilobase of exon per million fragments mapped (FPKM). Data was further analyzed and visualized using CummeRbund run under the R package (4.1.3). Statistical significance in differential gene expression between groups was assessed with Cuffdiff (2.1.1). Hierarchical clustering of genes was generated using

Complete Linkage as the clustering method. Euclidian distance was used as the similarity measure with Z-Score as the normalization method. These analyses were performed with TIBCO Spotfire Software (Palo Alto, CA). Pathway analysis was performed using Gene Set Enrichment Analysis (GSEA) (Broad Institute, software.broadinstitute.org/gsea), a computational method that determines statistical significance of a priori defined set of genes between two groups and ClueGo within Cytoscape software v3.10.3 using Kyoto Encyclopedia of Genes and Genomes (KEGG) pathways, WikiPathways (WP), Reactome pathways and Reactome reaction pathways, as well as GO biological process (GO BP). All RNA-seq studies were performed using samples derived from male WT and CF mice approximately 6-8 weeks of age. RNA-Seq data have been deposited in NCBI's Gene Expression Omnibus and are available through GSE291307.

Publicly available single cell RNA sequencing data

Publicly available single cell sequencing data for wildtype small intestine was used and analyzed with the 10X Genomics Loupe Browser v8.0.0 (11). Cell identity markers were determined using PanglaoDB and confirmed using a publicly available wildtype mouse small intestine spatial transcriptomics dataset Visium HD) (12, 13). Both the publicly available single cell and spatial transcriptomic datasets were pre-processed by 10X Genomics, including the normalization, dimensionality reduction/UMAP projection, and clustering (11, 13).

Quantification of intestinal layer thickness

Layer thickness was measured in the outer portion of Swiss rolls derived from the most proximal, central, and distal small intestinal segments to represent the duodenum, jejunum, and ileum respectively. Smooth muscle layer thickness (comprised of both circular and longitudinal layers) and length of complete villi and crypt units were measured using NDP.view v 2.7.52 software (Hamamatsu Photonics K.K). The smooth muscle to epithelial ratio was defined as the ratio of smooth muscle layer thickness (including both circular and longitudinal layers) over the combined villi and crypt length. Data are presented as mean ± SEM.

Ki67 Quantification

Slides were imaged on the Zeiss AxioObserver 7 fluorescence microscope on the 20x objective for best resolution and using the stitching feature to take a 2x2 image equivalent to a 10x field of view. The images were opened in QuPath and manually annotated to include only the crypts in the 10x field for analysis, leaving out positive immune cells in the villi. Ki67 staining was quantified using the positive cell detection tool in QuPath with the following settings: Detection channel AF594, requested pixel size 0.5μm, background radius 8μm, median filter radium 1.5 μm, minimum area 5μm^2, maximum area 200 μm^2, threshold 300, cell expansion 1T. Cell detection parameters were verified by a pathologist after QuPath cell detection was complete to ensure correct selection of positive cells.

Statistics

Data are reported as mean +/- standard error of the mean (SEM). Statistical analyses were performed using Student's t-tests as described in figure legends unless otherwise specified, using $p<0.05$ for determination of significance of differences. For repeated measurements, comparisons between groups were performed using a main effect repeated measures two-way ANOVA with the Geisser-Greenhouse correction. P-values are reported with the F statistic (degrees of freedom of the numerator, degrees of freedom of the denominator). The p-value for genotype is displayed on the relevant figures. Additional information is provided in the corresponding figure legends. For all figures $*p<0.05$, $**p<0.01$, $***p<0.001$, $****p< 0.0001$. Additional information regarding sample size, replicate numbers, and significance is included within the respective figure legends or corresponding method section. All figures were made using Graphpad Prism (10.3.0) and BioRender (https://BioRender.com).

RESULTS

Increased glucose uptake from circulation to CF intestine

While ^{18}F-Fluorodeoxyglucose (^{18}F-FDG), a radioactive glucose analog, has been extensively used to assess glucose uptake in various cancers, ^{18}F-FDG can also be leveraged for quantitative assessments of systemic *in vivo* glucose uptake from circulation to non-cancer cells and tissues (14). For instance, ^{18}F-FDG Positron Emission Tomography (PET) approaches have been used to study *in vivo* glucose uptake from the blood supply to intestine following gastric bypass surgeries and in inflammatory bowel disease (IBD) to provide insights into intestinal glucose demand, adaptive responses, and pathologic mechanisms (15–19). To assess systemic *in vivo*

glucose uptake from circulation, including intestinal glucose demand, ^{18}F-FDG PET/MRI studies were performed in wildtype (WT) and age and sex matched CF (G542X/G542X) mice (8). In short, mice were subject to a 4-hour fast prior to imaging to remove the confounding effects of food intake on label uptake. Next, mice were injected with ^{18}F-FDG through the tail vein and subsequently imaged with concurrent PET/MRI for visualization, localization, and quantification of label uptake. Interestingly, there was increased ^{18}F-FDG uptake from the blood supply to the CF intestine relative to WT (Figure 1A-C). No significant differences in *in vivo* glucose uptake were seen in the other organs examined, including the brain, heart, lung, kidney, liver, and skeletal muscle (Supplemental Figure S1).

Most pronounced increases in glucose uptake evident in CF jejunum and ileum

Our *in vivo* approaches indicated increased glucose uptake from circulation to the entire CF intestine, but could not differentiate between intestinal regions. Consequently, we performed *ex vivo* biodistribution studies to assess the localization of glucose uptake within the intestine. Following the *in vivo* ^{18}F-FDG PET/MRI study, duodenum, jejunum, ileum, and colon were removed and the radioactivity from the ^{18}F-FDG uptake was quantified. Consistent increases in signal from the ^{18}F-FDG were detected in the CF jejunum and ileum with each normalization method (Figure 2A-D). More variable increases in radioactivity were also seen in the CF duodenum and colon, but were dependent on normalization method and may suggest increased glucose uptake, but to a lesser extent (Figure 2A,D). Collectively, our *ex vivo* biodistribution

studies further localize the increased label uptake to the CF jejunum and ileum where the increases in radioactivity are most prominent.

Increased* Slc2a1 *(GLUT1) mRNA expression in CF intestinal tissue and isolated crypts

Next, we assessed glucose transporter gene expression through RNA Sequencing (RNA-Seq) studies on WT and CF duodenum, jejunum, ileum, and isolated crypts from the jejunum to identify the candidate transporter responsible for mediating the increased glucose uptake from circulation to the CF intestine. *Slc2a1* (GLUT1) was the only glucose transporter with consistently and significantly increased mRNA expression across all CF intestinal sections (Figure 3A-B, Supplemental Tables 1-4). The fold change in the CF duodenum was lower compared to CF jejunum and ileum and may account for the subtler, more variable elevation in glucose uptake seen in our biodistribution studies (Figure 3B, Supplemental Table 1). More sensitive approaches, including single cell RNA-Seq studies, confirm *Slc2a1* (GLUT1) gene expression in intestinal crypts and lower villi in WT small intestine and its differential localization from canonical luminal glucose transporters (Figure 3C, Supplemental Figure S2) (11).

There was also decreased gene expression of canonical luminal absorption glucose transporters (*Slc2a2* [GLUT2], *Slc5a1* [SGLT1]) in the CF jejunum, ileum, and isolated crypts (Figure 3A, Supplemental Tables 2-4). It is unclear if these decreases in gene expression translate into functional differences in luminal glucose absorption. There is not thought to be prominent carbohydrate malabsorption in CF (22, 23). Increased villi length, in addition to intestinal length, have been described in CF mouse

models and may also account for no functional difference in luminal carbohydrate absorption (24–26). While smooth muscle hypertrophy has been described in the CF ileum, there were not substantial differences in *Slc2a4* (GLUT4) mRNA expression, the prominent muscle glucose transporter between WT and CF intestinal sections (Figure 3B) (24). There was not appreciable mRNA expression of *Slc2a1* (GLUT1) in smooth muscle, as described below, suggesting a model of increased glucose by the epithelium and not the thickened smooth muscle.

Transcriptional enrichment of glycolysis in CF intestine

To determine if there were also differences in glucose metabolism, in addition to the increased glucose uptake in the CF intestine, we revisited our RNA-Seq studies to identify pathways of interest pertaining to glucose utilization. Numerous differentially enriched pathways were identified in the CF intestine (Supplemental Figures S3-S6). The glycolysis pathway was one of the top hits and enriched in the CF jejunum, ileum, and isolated crypts (Figure 4A-B, Supplemental Figures S4-S6). More specifically, there was significantly increased expression of most glycolytic genes with good concordance across CF jejunum, ileum, and jejunal crypts samples (Figure 4D-E, Supplemental Tables 2-4). Enrichment of glycolysis within the isolated crypts, suggests that the crypts are contributing, at least in part, to the elevated glycolysis seen in the whole tissue. There was not a statistically significant enrichment of the glycolysis pathway in the CF duodenum compared to WT (Figure 4B). While only 2 genes from the glycolysis pathway (*Hk2* and *Aldoa*) were significantly increased in the CF duodenum, the expression of the majority of glycolytic genes was increased in CF relative to the WT,

indicating there may be a similar, but more subtle effect in the duodenum (Figure 4D-E, Supplemental Table 1). Additionally, there were numerous alterations in pathways beyond glycolysis, which merit further investigation in subsequent work (Supplemental Figures S3-S6). Overall, there is a transcriptional enrichment of the glycolysis pathway in the CF intestine, particularly, the jejunum, ileum, and isolated crypts.

Increased GLUT1 and HK2 protein expression in CF intestinal tissue and isolated crypts

To ascertain if the gene expression differences translated to protein level differences, we assessed GLUT1 and Hexokinase2 (HK2) protein expression in both intestinal isolated crypts and whole intestinal tissue. Increased GLUT1 expression was seen in whole tissue and isolated crypts from the CF jejunum and ileum compared to WT controls (Figure 5A,C). Similarly, increased HK2 expression was detected in the CF jejunum and ileum whole tissue, in addition to isolated crypts (Figures 5B,D). Increased GLUT1 and HK2 protein expression in the CF intestinal crypts may suggest an increased glucose demand for the crypts themselves, in addition to the whole tissue. In the duodenum, there was relatively similar GLUT1 expression in WT and CF whole tissue and crypts with increased HK2 expression particularly evident in the CF crypts (Figure 5A-D). These findings are consistent with the more variable glucose uptake and less prominent gene expression changes seen in the duodenum. Conversely, more pronounced increases in GLUT1 and HK2 protein expression were seen in the CF jejunum and ileum where there was also greater enrichment of glycolytic gene expression and more robust increases in glucose uptake.

Increased functional glycolysis in CF intestine

Next, we sought to test functional differences in glycolysis. Basal extracellular acidification rate (ECAR) was measured in WT and CF duodenum, jejunum, and ileum. Lactate media levels were also quantified to confirm that the changes in ECAR were coming from altered glycolysis (Figure 6G). No differences in oxygen consumption rates (OCR) were found between WT and CF duodenum, jejunum, and ileum (Supplemental Figure S7). However, further assay optimization is required to fully interrogate oxygen consumption due to the presence of multiple possible substrate sources within the assay media, which may compensate for additional impairments in macronutrient metabolism and mitochondrial function.

Increased ECAR was seen in both CF jejunum and ileum samples compared to WT controls (Figure 6C-F). Corresponding increases in lactate concentration were observed in the media of CF jejunum and ileum samples compared to WT (Figure 6H). Collectively, these findings of increased ECAR with corresponding lactate elevations indicate an increase in functional glycolysis in CF jejunum and ileum-derived samples. There were no differences in ECAR between WT and CF duodenum tissue samples (Figure 6A-B). Additionally, there were similar media lactate levels between WT and CF duodenum samples, indicating that there was not a difference in functional glycolysis (Figure 6H). Overall, the most prominent increases in functional glycolysis were in the CF jejunum and ileum, consistent with the glucose uptake and RNA-Seq findings.

Evidence of proliferative adaptations in CF intestine

In order to assess the mechanisms underlying the increased intestinal glucose uptake and metabolism phenotype in CF, we examined the morphologic features of the CF intestine. Intriguingly, we observed significantly increased absolute and relative intestinal length and weight in CF mice (Figure 7A-E). The difference in absolute intestinal length was due to increased small intestine length in CF, which has also been previously described in another CF mouse model (25). We also noted increased weight of each part of small intestine in CF, in addition to increased gross diameter (Supplemental Figure S8C-G). Increased intestinal diameter and length indicate an increased intestinal surface area that is likely an adaptation to increase nutrient absorption.

In addition to gross morphologic changes, we also assessed intestinal histology. Increased crypt depth and villus length were observed throughout the CF small intestines compared to WT (Figure 8 A-M). Smooth muscle thickness was increased in the CF jejunum and ileum (Figure 8 M-N). The CF ileum had the most dramatic increase in the smooth muscle thickness evident through the approximately 2-fold increase in the smooth muscle to epithelial ratio compared to WT (Figure 8 M-N). The increased smooth muscle thickness in the CF jejunum was statistically significant, but smaller in magnitude compared to the changes in the ileum. There was no evidence of tissue damage nor substantial immune cell infiltrates in the CF intestine.

Spatial detection of Slc2a1 and Hk2 in epithelia

To assess the spatial localization of *Hk2* and *Slc2a1* gene expression, RNAscope was used to detect mRNA from the respective genes (Figure 9 A-L,

Supplemental Figure S9). In all intestinal sections, staining was most prominent in the CF crypts and villi. More intense staining was evident in the CF jejunum and ileum (Figure 9E-L). A slight increase in *Hk2* and *Slc2a1* expression can be seen in the CF duodenal crypts (Figure 9 C-D). Staining of mRNA for either gene in smooth muscle of all sections was nearly undetectable (Supplemental Figure S9). Taken together, increased *Slc2a1* and *Hk2* expression was most apparent in the CF jejunum and ileum and evident in both the crypt and villus regions.

Increased cell proliferation in CF intestines

Increased glycolysis could reflect energy demands of cell proliferation. As smooth muscle, crypts and villi are enlarged in CF, intestinal tissue sections were stained for the cell proliferation marker Ki67 (Figure 10A-F). Positively stained cells were apparent in the crypts and lower villus regions with higher numbers in the CF duodenum, jejunum and ileum, compared to WT, as shown in Figure 10G.

DISCUSSION

Herein, we report the novel findings of increased intestinal glucose uptake from circulation and increased glycolysis in a CF mouse model through complementary transcriptional, protein, and functional approaches. Increased *in vivo* glucose uptake from circulation to the CF intestines was observed with the most robust increases detected in the CF jejunum and ileum. GLUT1, as the only glucose transporter found to be increased, likely mediates the observed elevated glucose uptake. Elevated glycolysis was also seen on the transcriptional and functional levels in the CF jejunum and ileum.

Importantly, the altered intestinal glucose metabolism was seen in the context of hyperplastic histologic and morphologic changes in the CF intestine and suggestive of increased intestinal glucose demand due to an adaptive response.

The intestine is a uniquely flexible organ capable of undergoing adaptive changes depending on a variety of factors, including nutritional, hormonal, neural, immune, mechanical, morphologic, and developmental stimuli within the intestinal environment (27). Intestinal adaptations can be atrophic or proliferative in nature. Mucosal atrophy occurs with starvation or the lack of luminal contents in the case of total parenteral nutrition (27–29). Atrophic adaptations include decreased villus height, crypt depth, surface area, in addition to decreased intestinal weight (27–29). Conversely, proliferative adaptive responses arise as a compensatory mechanism to impaired intestinal function (27). Proliferative adaptations have been described following small bowel resection and malabsorptive bariatric surgeries, such as Roux-en-Y Gastric Bypass (RYGB) surgery (15, 16, 27, 30). These adaptive responses are comprised of increased villi length, crypt depth, and surface area (15, 27, 30). These proliferative adaptive changes are similar to what has been described in the CF intestine in this study and by others (24–26).

In particular, increased crypt depth, villus length, smooth muscle hypertrophy, and goblet cell hyperplasia with preservation of tissue architecture have been consistently documented in the ileum across multiple CF mouse models (24–26). Our histology findings are in agreement with these established findings. Additionally, we identified similar hyperplastic, histologic changes in the CF jejunum and to a lesser extent in the duodenum. Increased small intestinal length and weight in CF were also

observed. Overall, these morphologic and histologic changes are suggestive of a proliferative adaptive response in the CF intestine.

The hyperplastic changes in the CF intestine were seen in the context of increased intestinal glucose uptake from the circulation. We detected a consistent pattern of increased *Slc2a1* gene and GLUT1 protein expression in both CF intestinal tissue and isolated crypts. GLUT1 is thought to be minimally expressed in the adult small intestine in rodents and humans under basal conditions (15, 16, 20, 21). However, intestinal GLUT1 expression is increased in various adaptive or pathologic states with increased intestinal proliferation, such as following Roux-en-Y gastric bypass (RYGB) surgery or gastrointestinal cancer (15, 16, 31–33). GLUT1 elevations in these conditions similarly facilitate increased glucose uptake from the blood supply to intestine as we observed in our study (15, 16, 33, 34). Thus, GLUT1 emerged as a strong candidate transporter for mediating the increased intestinal glucose uptake from circulation in CF. RNAscope further localizes the site of the effect to the epithelium.

Elevated glycolysis was also evident in the CF intestine, in addition to increased glucose uptake. Transcriptional and functional increases in glycolysis were most prominent in the CF jejunum and ileum where the increases in glucose uptake were most robust. Increased glycolysis is a metabolic means of providing anabolic and energetic substrates to facilitate increased proliferative demands (15, 35). Evidence of increased glucose uptake and glycolysis was seen in both whole tissue and isolated crypts. These findings suggest that the crypts partially contribute to the increased glucose utilization in the CF intestine. Taken together, the increased glucose demand

574 and glycolysis in the CF intestine reflect metabolic changes to maintain intestinal
575 homeostasis.
576 The CF intestine shares striking similarities with the proliferative intestinal
577 adaptations seen following RYGB surgery. RYGB is a surgical method that restricts
578 food intake and decreases nutrient absorption to promote weight loss through both
579 surgical reduction of the stomach and direct connection to the stomach. This new
580 stomach-jejunum connection is termed the “Roux limb.” Thus, ingested food bypasses
581 the majority of the stomach and duodenum and enters directly into the jejunum relatively
582 undigested. The duodenum is surgically connected to the Roux limb to create a
583 “common limb” to deliver various digestive juices and pancreatic enzymes to ingested
584 food in the intersection of the limbs.
585 As in our study, RYGB surgery results in increased intestinal glucose uptake
586 from circulation seen with ^{18}F-FDG imaging, increased mRNA and protein levels of
587 GLUT1 and HK2, increased gene and protein expression of glycolysis enzymes, and
588 hyperplastic morphologic and histologic intestinal changes (15, 34). These pro-
589 proliferative histologic changes and elevated glucose uptake and glycolysis are only
590 seen in the Roux and common limbs, which contain undigested food (15, 16).
591 Additionally, increases in proliferation markers, such as Ki67 and PCNA, have been
592 documented in the intestine following RYGB surgery and in CF (15, 16, 25, 26, 36).
593 With RYGB, the increased GLUT1 mediated intestinal glucose uptake and the
594 concomitant increases in glycolysis are necessary to maintain the anabolic and
595 energetic demands of increased proliferation and tissue mass following RYGB surgery
596 (15, 16). The increased intestinal glucose demand contributes, at least in part, to the

decreased blood glucose seen following RYGB surgery (15, 34). While a Cystic Fibrosis-Related Diabetes phenotype is not apparent in CF mice, there have been reports of unexpected decreased circulating blood glucose in CF mouse models (26, 37). Our results suggest the CF intestine is similarly consuming a portion of this circulating glucose. The many apparent parallels between the CF intestine and after RYGB surgery suggest there may be similar increases in intestinal glucose demand and adaptive responses.

While the exact mechanisms underlying intestinal proliferative adaptations are still unclear, the presence of undigested food is thought to play a role after RYGB surgery (15). Undigested food may also be of relevance in CF, albeit in a different context. Decreased pancreatic exocrine function, defects in biliary system and function, increased mucus production, altered pH, decreased digestive enzyme activity, smooth muscle contractile dysfunction, dysmotility, and dysbiosis contribute to impaired digestion and absorption in CF (2, 6, 7). We propose that these complex and multifactorial digestive and absorptive defects in CF contribute to incomplete digestion that creates an intestinal environment functionally similar to the undigested nutrients following RYGB surgery. Thus, there is an adaptive need in CF to increase nutrient absorption and allow for more time for digestion. Consequently, there is an adaptive hyperproliferative response in the CF intestine. These adaptations include increased crypt depth and villus length, in addition to increased intestinal length, diameter, and weight to ultimately increase the absorptive surface area of the CF intestine. Consequently, there is increased intestinal glucose demand to maintain proliferation and intestinal homeostasis in CF.

There are numerous alternative mechanisms for increased basolateral glucose uptake and metabolism in the CF intestine that merit further investigation. These include mitochondrial dysfunction, impaired lipid utilization, metabolic adaptations to dysfunctional CFTR, decreased luminal carbohydrate absorption or diversion of dietary glucose for other fates, microbiome differences, inflammation, hypoxic or stress response, additional environmental factors, such as altered hormones and signaling differences (17, 19, 38-40). While there is some existing supportive evidence for many of these factors, the exact mechanisms and relevance pertaining to CF intestinal disease remain unclear. Each alternative explanation merits further investigation as a contributing factor to CF intestinal pathogenesis in its own right and in conjunction with other potential mechanisms of disease. For instance, many uncertainties remain with regards to the potential role and mechanisms of mitochondrial dysfunction in CF related to electron transport chain complexes involved, cell type and tissue specificity, direct role for CFTR in regulating mitochondrial homeostasis or indirect effect of dysfunctional CFTR related to the CF environment (38, 41–43).

Similarly, increased glucose uptake and glycolysis by immune cells is another possible alternative explanation. While mild, chronic inflammation is often described in potential mechanisms of CF intestinal pathogenesis, the degree of inflammation, cell types responsible, and sources still remain unclear (24, 26, 39, 44). Studies of the CF mouse intestinal histology have reported differing findings with respect to immune cells. Some groups show no evidence of significant immune infiltrates, while others report an increased number of mast cells or neutrophils in the ileum (24, 26, 39). We did not see evidence of significant immune infiltration or tissue injury on histologic evaluation. Our

morphologic and histology findings in the context of the diffuse intestinal ^{18}F-FDG uptake in the CF intestine are comparable to the hyperplastic adaptive changes seen following RYGB surgery, which are indicative of increased tissue mass and proliferation. Importantly, our findings contrast with inflammation in the setting of IBD models, which present with patchy, focal areas of increased intestinal ^{18}F-FDG uptake that directly correspond to areas of substantial immune infiltrate and tissue injury on histology (17, 19). Taken together, the CF intestine more closely resembles the established proliferative adaptive response and increased glucose demand seen after RYGB surgery.

Our biodistribution, RNA-Seq, protein expression, and functional studies are in agreement. Collectively, these approaches identified the most pronounced increases in glucose uptake from the blood supply and glycolysis in the CF jejunum and ileum. It is currently unclear why the glucose metabolism changes were less prominent in the CF duodenum. The CF duodenum could have a greater reliance on other macronutrients to maintain potential intestinal adaptations. Smooth muscle differences could also contribute to differential glucose uptake in CF. Increased smooth muscle thickness was observed in the CF jejunum and ileum. The smooth muscle layer was considerably more pronounced in the CF ileum compared to the CF jejunum. Yet, similar magnitudes of increased ECAR were observed in both regions. Furthermore, glycolytic gene expression enrichment in isolated crypts and spatial data showing elevated expression of *Slc2a1* and *Hk2* in villi, along with increased GLUT1 and HK2 protein expression suggests that intestinal epithelial cells contribute at least in part to the increased glucose metabolism in CF. Smooth muscle differences may partially contribute to

increased glucose uptake in the CF intestine, but are unlikely the driving force. Future studies are necessary to assess regional specific intestinal adaptive mechanisms and the contribution of multiple fuel sources. While there has been some early studies exploring a direct role of CFTR in intestinal stem cells, more work is also needed to determine how broader deficits in digestion and absorption in the context of the CF environment also contribute to increased intestinal cell proliferation and disease pathogenesis (25, 45, 46).

Our findings and proposed mechanism put forth a new perspective to studying the intestinal manifestations of CF. Future work should determine the utility of ^{18}F-FDG imaging approaches for assessing intestinal disease in people with CF in relation to intestinal symptoms and GI cancer development. Additional efforts should explore how proliferative intestinal adaptations and elevated glycolysis may also contribute to the increased risk of gastrointestinal cancer in CF. Existing therapies may be insufficiently targeting the extent of digestive and absorptive deficits in CF. Current modulator therapy remains less effective for the gastrointestinal manifestations of CF and additional therapeutic approaches that improve digestion and absorption may also enhance modulator efficacy and uniformity in response. Taken together, our findings improve our understanding of CF intestinal pathogenesis and set the foundation for future work to elucidate additional disease mechanisms and novel therapeutic approaches for treating the GI manifestations of CF.

ACKNOWLEDGEMENTS

The authors would like to thank the Cystic Fibrosis Mouse Resource Center, in particular Dr. Craig Hodges, Dr. Amanda Barabas, Sakeena Davis, and Molly Schneider, for providing the animals used for this study. The authors also acknowledge the assistance of the Case Western Reserve University School of Medicine Imaging Research Facility and the support of the Case Western Reserve University School of Medicine's Research Institute for Children's Health. Figure 4C and the graphical abstract were created in BioRender (Lesser, A. ((2025)) https://BioRender.com/p29d101).

Funding statement

This work was supported by Cystic Fibrosis Foundation grants DRUMM24R0 (MLD) and DRUMM22G0-GI (MLD), T32 GM152319 (AFL) and S10OD03049901 (CAF).

Supplemental Material

Supplemental Figures 1-9, Supplemental Tables 1-4:
https://doi.org/10.6084/m9.figshare.29613872

Figure Legends:

Figure 1: Increased *in vivo* glucose uptake from the blood supply to CF intestine.
Quantification of ^{18}F-FDG intestinal uptake from the blood supply in WT (n=7) and CF (n=8) mice using PET/MRI (A). Representative images from CF (B) and WT mice (C).

The heart is labeled in white with thin arrows and the intestine is labeled in yellow with thick arrows. Data represent mean ± SEM. Comparisons between groups were performed using a repeated measures two-way ANOVA with the Geisser-Greenhouse correction. The p-value for genotype is displayed where p=0.0243, F (1, 13) = 6.489. For time, p<0.0001, F (1.423, 19.92) = 67.91. * p<0.05.

Figure 2: Increased glucose uptake in CF jejunum and ileum. Biodistribution study quantifying the radioactivity in the respective parts of the intestine normalized to wet weight (A), wet weight with stool contents removed (B), dry weight (C), and radioactivity (Mbq)/g dry weight (D) in WT (n=6-7) and CF (n=7-8) mice. Data represent mean ± SEM. Comparison between groups for each intestinal region were performed using an unpaired, 2-tailed Student's *t* test with Welch's correction. * p<0.05, ** p<0.01.

Figure 3: Increased *Slc2a1* (GLUT1) mRNA expression in CF intestine. Heatmaps showing significant changes in gene expression (A) and Log2 Fold Change (B) for key glucose transporter genes from RNA Sequencing (RNA-Seq) studies from WT and CF duodenum, jejunum, ileum, and crypts isolated from the jejunum (Jej) (WT n=4-9, CF n=5-9). UMAP (Uniform Manifold Approximation Projection) plots displaying single cell RNA-Seq data from wildtype mouse small intestine using publicly available dataset for select glucose transporter genes (C). Gray cells on the UMAP plots indicate that the relevant transcript was not detected. Significance was defined as q<0.05 for RNA-Seq studies.

Figure 4: Enrichment of glycolysis pathway in CF jejunum, ileum, and isolated crypts. Top 20 significantly increased pathways in the CF jejunum (A). Glycolysis pathway enrichment from RNA-Seq studies of WT and CF duodenum, jejunum, ileum, and isolated crypts from the jejunum (Jej) (WT n=4-9, CF n=5-9) (B). Glycolysis pathway (C). Heatmaps showing significant changes in mRNA expression for glycolysis genes (D) and Log2 Fold Change (E). Significance was defined as $q<0.05$ for gene expression and corrected $p<0.05$ for pathway analysis from Kyoto Encyclopedia of Genes and Genomes (KEGG), WikiPathways (WP), Reactome pathways, Reactome reaction pathways, and GO biological process (GO BP) glycolysis related terms.

Figure 5: Increased GLUT1 and HK2 protein expression in CF jejunum, ileum, and isolated crypts. Western blot analysis of GLUT1 and HK2 protein expression from intestinal whole tissue (A,B) and isolated crypts (C,D) from duodenum, jejunum, and ileum of WT (n=2) and CF (n=2) mice. The arrow indicates the expected HK2 band size of 102 kDa.

Figure 6: Increased functional glycolysis in CF jejunum and ileum. Extracellular Acidification Rate (ECAR) from duodenum (A-B), jejunum (C-D), and ileum (E-F) *ex vivo* intestinal biopsy punches derived from WT (n=7-11) and CF (n=7-11) mice. Data presented as average over the course of 10 measurements (A, C, E) and cumulative average per mouse (B, D, F). Simplified glycolysis pathway (G). Media lactate measurements from *ex vivo* intestinal biopsy punches presented as fold change relative to wildtype within the respective intestinal regions from WT (n=6) and CF (n=6) mice

(H). Data represent mean ± SEM. Comparisons between groups were performed using an unpaired, 2-tailed Student's t test with Welch's correction or using a repeated measures two-way ANOVA with the Geisser-Greenhouse correction. For repeated measurements, the p-value for genotype is displayed and was found to be $p<0.0001$, $F(1, 20) = 26.63$ for the jejunum and $p<0.0001$, $F(1, 12) = 56.06$ for the ileum. There was not a significant difference for genotype in the duodenum, $p=0.2821$, $F(1, 12) = 1.268$. For time, $F(1.017, 13.22) = 238.2$, $p<0.0001$ for the duodenum, $F(1.107, 23.24) = 2.910$, $p=0.0983$ for the jejunum, and $F(1.365, 17.74) = 6.047$, $p=0.0171$ for the ileum. * $p<0.05$, ** $p<0.01$, ***$p<0.001$, **** $p<0.0001$.

Figure 7: Morphologic and histologic changes in the CF intestine. Intestine length (A), intestinal wet weight (B), body weight (C) in WT (n=7-15) and CF (n=8-15) mice. Intestinal length (D) and wet weight (E) normalized to body weight. Data represent mean ± SEM. Comparisons between groups were performed using an unpaired, 2-tailed Student's *t* test with Welch's correction. ****$p<0.0001$.

Figure 8: Histologic changes in the CF intestine. Representative images of WT and CF intestinal histology for duodenum (A-D), jejunum, (E-H), and ileum (I-L). Quantification of villi length, crypt depth, and smooth muscle thickness from intestinal histology samples from WT (n=13) and CF (n=21) mice (M). Smooth muscle to epithelial ratio where epithelial is defined as the sum of villi length and crypt depth (N). Data represent mean ± SEM. Comparisons between groups were performed using an unpaired, 2-tailed Student's *t* test with Welch's correction. ***$p<0.001$.

Figure 9: Increased *Slc2a1* (GLUT1) and *Hk2* mRNA expression in the CF intestine. Representative RNAscope images from WT and CF duodenum (A-D), jejunum (E-H), and ileum (I-L). Representative images include both intestinal villi (A-B, E-F, I-J) and crypts (C-D, G-H, K-L) for each segment.

Figure 10: Increased Ki67 positive cells in the CF intestine. Representative images from WT and CF duodenum (A-B), jejunum (C-D), and ileum (E-F). Quantification of Ki67 positive cell counts per 10X magnification field from WT (n=6) and CF (n=5) mice (G). Data represent mean ± SEM. Comparisons between groups were performed using an unpaired, 2-tailed Student's *t* test with Welch's correction. *p<0.05. ** p<0.01, ****p<0.0001.

1. **Calthorpe RJ**, **Goodchild N**, **Gleetus V**, **Premakumar V**, **Hayee B**, **Elliott Z**, **Evans B**, **Rowbotham NJ**, **Carr SB**, **Barr H**, **Horsley A**, **Peckham D**, **Smyth AR**. A grumbling concern: A survey of gastrointestinal symptoms in cystic fibrosis in the modulator era. *NIHR Open Res* 3: 18, 2024. doi: 10.3310/NIHROPENRES.13384.2.
2. **Ooi CY**, **Durie PR**. Cystic fibrosis from the gastroenterologist's perspective. *Nat Rev Gastroenterol Hepatol 2016 133* 13: 175–185, 2016. doi: 10.1038/nrgastro.2015.226.
3. **Maisonneuve P**, **Marshall BC**, **Knapp EA**, **Lowenfels AB**. Cancer Risk in Cystic Fibrosis: A 20-Year Nationwide Study From the United States. *JNCI J Natl Cancer Inst* 105: 122–129, 2013. doi: 10.1093/JNCI/DJS481.
4. **Yamada A**, **Komaki Y**, **Komaki F**, **Micic D**, **Zullow S**, **Sakuraba A**. Risk of gastrointestinal cancers in patients with cystic fibrosis: a systematic review and meta-analysis. *Lancet Oncol* 19: 758–767, 2018. doi: 10.1016/S1470-2045(18)30188-8.
5. **Hadjiliadis D**, **Khoruts A**, **Zauber AG**, **Hempstead SE**, **Maisonneuve P**, **Lowenfels AB**, **Braid AL**, **Cullina J**, **Daggett A**, **Fink A**, **Gini A**, **Harron PF**, **Lansdorp-Vogelaar I**, **Lieberman D**, **Liou T**, **Lomas P**, **Marshall B**, **Meyer K**, **Rustgi A**, **Shaukat A**, **Sabadosa K**. Cystic Fibrosis Colorectal Cancer Screening Consensus Recommendations. *Gastroenterology* 154: 736-745.e14, 2018. doi: 10.1053/j.gastro.2017.12.012.
6. **De Lisle RC**, **Borowitz D**. The Cystic Fibrosis Intestine. *Cold Spring Harb Perspect Med* 3, 2013. doi: 10.1101/CSHPERSPECT.A009753.
7. **Li L**, **Somerset S**. Digestive system dysfunction in cystic fibrosis: Challenges for nutrition therapy. *Dig Liver Dis* 46: 865–874, 2014. doi: 10.1016/J.DLD.2014.06.011.
8. **McHugh DR**, **Steele MS**, **Valerio DM**, **Miron A**, **Mann RJ**, **LePage DF**, **Conlon RA**, **Cotton CU**, **Drumm ML**, **Hodges CA**. A G542X cystic fibrosis mouse model for examining nonsense mutation directed therapies. *PLoS One* 13: e0199573, 2018. doi: 10.1371/JOURNAL.PONE.0199573.
9. **Fan L**, **Lesser AF**, **Sweet DR**, **Keerthy KS**, **Lu Y**, **Chan ER**, **Vinayachandran V**, **Ilkayeva O**, **Das T**, **Newgard CB**, **Jain MK**. KLF15 controls brown adipose tissue transcriptional flexibility and metabolism in response to various energetic demands. *iScience* 25, 2022. doi: 10.1016/J.ISCI.2022.105292.
10. **Williams JM**, **Duckworth CA**, **Vowell K**, **Burkitt MD**, **Pritchard DM**. Intestinal Preparation Techniques for Histological Analysis in the Mouse. *Curr Protoc Mouse Biol* 6: 148–168, 2016. doi: 10.1002/CPMO.2.
11. 40k Mixture of Cells Dissociated from 4 Fixed Mouse Tissues using gentleMACS Dissociator, Multiplexed Samples, 4 Probe Barcodes (Next GEM), Flex Gene Expression dataset analyzed using Cell Ranger 7.1.0, 10X Genomics. 2022.
12. **Oscar Franzén, Li-Ming Gan JLMB**. PanglaoDB: a web server for exploration of mouse and human single-cell RNA sequencing data. Volume 2019, 2019.
13. Visium HD Spatial Gene Expression Library, Mouse Small Intestine (FFPE) - 10x Genomics. 2024.
14. **Almuhaideb A**, **Papathanasiou N**, **Bomanji J**. 18F-FDG PET/CT Imaging In Oncology. *Ann Saudi Med* 31: 3–13, 2011. doi: 10.4103/0256-4947.75771.

15. **Saeidi N**, **Meoli L**, **Nestoridi E**, **Gupta NK**, **Kvas S**, **Kucharczyk J**, **Bonab AA**, **Fischman AJ**, **Yarmush ML**, **Stylopoulos N**. Reprogramming of intestinal glucose metabolism and glycemic control in rats after gastric bypass. *Science (80-)* 341: 406–410, 2013. doi: 10.1126/SCIENCE.1235103/SUPPL_FILE/SAEIDI-SM.PDF.
16. **Cavin JB**, **Couvelard A**, **Lebtahi R**, **Ducroc R**, **Arapis K**, **Voitellier E**, **Cluzeaud F**, **Gillard L**, **Hourseau M**, **Mikail N**, **Ribeiro-Parenti L**, **Kapel N**, **Marmuse JP**, **Bado A**, **Le Gall M**. Differences in Alimentary Glucose Absorption and Intestinal Disposal of Blood Glucose After Roux-en-Y Gastric Bypass vs Sleeve Gastrectomy. *Gastroenterology* 150: 454-464.e9, 2016. doi: 10.1053/J.GASTRO.2015.10.009.
17. **Hindryckx P**, **Staelens S**, **Devisscher L**, **Deleye S**, **De Vos F**, **Delrue L**, **Peeters H**, **Laukens D**, **De Vos M**. Longitudinal quantification of inflammation in the murine dextran sodium sulfate-induced colitis model using μPET/CT. *Inflamm Bowel Dis* 17: 2058–2064, 2011. doi: 10.1002/IBD.21578.
18. **Treglia G**, **Quartuccio N**, **Sadeghi R**, **Farchione A**, **Caldarella C**, **Bertagna F**, **Fania P**, **Cistaro A**. Diagnostic performance of Fluorine-18-Fluorodeoxyglucose positron emission tomography in patients with chronic inflammatory bowel disease: A systematic review and a meta-analysis. *J Crohn's Colitis* 7: 345–354, 2013. doi: 10.1016/J.CROHNS.2012.08.005/2/7-5-004.JPEG.
19. **Bettenworth D**, **Reuter S**, **Hermann S**, **Weckesser M**, **Kerstiens L**, **Stratis A**, **Nowacki TM**, **Ross M**, **Lenze F**, **Edemir B**, **Maaser C**, **Pap T**, **Koschmieder S**, **Heidemann J**, **Schafers M**, **Lugering A**. Translational 18F-FDG PET/CT Imaging to Monitor Lesion Activity in Intestinal Inflammation. *J Nucl Med* 54: 748–755, 2013. doi: 10.2967/JNUMED.112.112623.
20. **Yoshikawa T**, **Inoue R**, **Matsumoto M**, **Yajima T**, **Ushida K**, **Iwanaga T**. Comparative expression of hexose transporters (SGLT1, GLUT1, GLUT2 and GLUT5) throughout the mouse gastrointestinal tract. *Histochem Cell Biol* 135: 183–194, 2011. doi: 10.1007/S00418-011-0779-1/FIGURES/8.
21. **Boyer S**, **Sharp PA**, **Debnam ES**, **Baldwin SA**, **Srai SKS**. Streptozotocin diabetes and the expression of GLUT1 at the brush border and basolateral membranes of intestinal enterocytes. *FEBS Lett* 396: 218–222, 1996. doi: 10.1016/0014-5793(96)01102-7.
22. **Hoffman RD**, **Isenberg JN**, **Powell GK**. Carbohydrate malabsorption is minimal in school-age cystic fibrosis children. *Dig Dis Sci* 32: 1071–1074, 1987. doi: 10.1007/BF01300190.
23. **Grubb BR**. Ion transport across the jejunum in normal and cystic fibrosis mice. *Am J Physiol - Gastrointest Liver Physiol* 268: G505–G513, 1995. doi: 10.1152/AJPGI.1995.268.3.G505.
24. **Bazett M**, **Honeyman L**, **Stefanov AN**, **Pope CE**, **Hoffman LR**, **Haston CK**. Cystic fibrosis mouse model-dependent intestinal structure and gut microbiome. *Mamm Genome* 26: 222–234, 2015. doi: 10.1007/S00335-015-9560-4/TABLES/1.
25. **Liu K**, **Wang X**, **Zou C**, **Zhang J**, **Chen H**, **Tsang L**, **Yu MK**, **Chung YW**, **Wang J**, **Dai Y**, **Liu Y**, **Zhang X**. Defective CFTR promotes intestinal proliferation via inhibition of the hedgehog pathway during cystic fibrosis. *Cancer Lett* 446: 15–24, 2019. doi: 10.1016/J.CANLET.2018.12.018.

26. **Canale-Zambrano JC**, **Poffenberger MC**, **Cory SM**, **Humes DG**, **Haston CK**. Intestinal phenotype of variable-weight cystic fibrosis knockout mice. *Am J Physiol - Gastrointest Liver Physiol* 293, 2007. doi: 10.1152/ajpgi.00405.2006.
27. **Shaw D**, **Gohil K**, **Basson MD**. Intestinal mucosal atrophy and adaptation. *World J Gastroenterol* 18: 6357, 2012. doi: 10.3748/WJG.V18.I44.6357.
28. **Niinikoski H**, **Stoll B**, **Guan X**, **Kansagra K**, **Lambert BD**, **Stephens J**, **Hartmann B**, **Holst JJ**, **Burrin DG**. Onset of Small Intestinal Atrophy Is Associated with Reduced Intestinal Blood Flow in TPN-Fed Neonatal Piglets. *J Nutr* 134: 1467–1474, 2004. doi: 10.1093/JN/134.6.1467.
29. **Song J**, **Wolf SE**, **Wu XW**, **Finnerty CC**, **Gauglitz GG**, **Herndon DN**, **Jeschke MG**. Starvation-Induced Proximal Gut Mucosal Atrophy Diminished With Aging. *J Parenter Enter Nutr* 33: 411–416, 2009. doi: 10.1177/0148607108325178.
30. **Warner BW**. The Pathogenesis of Resection-Associated Intestinal Adaptation. *Cell Mol Gastroenterol Hepatol* 2: 429–438, 2016. doi: 10.1016/J.JCMGH.2016.05.001.
31. **Matsumoto K**, **Takao Y**, **Akazawa S**, **Yano M**, **Uotani S**, **Kawasaki E**, **Takino H**, **Yamasaki H**, **Okuno S**, **Yamaguchi Y**, **Nagataki S**. Developmental Change of Facilitative Glucose Transporter Expression in Rat Embryonal and Fetal Intestine. *Biochem Biophys Res Commun* 193: 1275–1282, 1993. doi: 10.1006/BBRC.1993.1763.
32. **Yamamoto T**, **Seino Y**, **Fukumoto H**, **Koh G**, **Yano H**, **Inagaki N**, **Yamada Y**, **Inoue K**, **Manabe T**, **Imura H**. Over-expression of facilitative glucose transporter genes in human cancer. *Biochem Biophys Res Commun* 170: 223–230, 1990. doi: 10.1016/0006-291X(90)91263-R.
33. **Haber RS**, **Rathan A**, **Weiser KR**, **Pritsker A**, **Itzkowitz SH**, **Bodian C**, **Slater G**, **Weiss A**, **Burstein DE**. GLUT1 glucose transporter expression in colorectal carcinoma: a marker for poor prognosis. *Cancer* 83: 34–40, 1998. doi: 10.1002/(sici)1097-0142(19980701)83:1<34::aid-cncr5>3.0.co;2-e.
34. **Oh JH**, **Kang CW**, **Wang EK**, **Nam JH**, **Lee S**, **Park KH**, **Lee EJ**, **Cho A**, **Ku CR**. Altered Glucose Metabolism and Glucose Transporters in Systemic Organs After Bariatric Surgery. *Front Endocrinol (Lausanne)* 13: 937394, 2022. doi: 10.3389/FENDO.2022.937394/BIBTEX.
35. **Lunt SY**, **Vander Heiden MG**. Aerobic glycolysis: Meeting the metabolic requirements of cell proliferation. *Annu Rev Cell Dev Biol* 27: 441–464, 2011. doi: 10.1146/ANNUREV-CELLBIO-092910-154237/CITE/REFWORKS.
36. **Maiuri L**, **Raia V**, **De Marco G**, **Coletta S**, **De Ritis G**, **Londei M**, **Auricchio S**. DNA fragmentation is a feature of cystic fibrosis epithelial cells: a disease with inappropriate apoptosis? *FEBS Lett* 408: 225–231, 1997. doi: 10.1016/S0014-5793(97)00347-5.
37. **Fontés G**, **Ghislain J**, **Benterki I**, **Zarrouki B**, **Trudel D**, **Berthiaume Y**, **Poitout V**. The ΔF508 Mutation in the Cystic Fibrosis Transmembrane Conductance Regulator Is Associated With Progressive Insulin Resistance and Decreased Functional β-Cell Mass in Mice. *Diabetes* 64: 4112–4122, 2015. doi: 10.2337/DB14-0810.
38. **Valdivieso AG**, **Santa-Coloma TA**. CFTR activity and mitochondrial function. *Redox Biol* 1: 190–202, 2013. doi: 10.1016/J.REDOX.2012.11.007.

39. **Norkina O**, **Kaur S**, **Ziemer D**, **De Lisle RC**. Inflammation of the cystic fibrosis mouse small intestine. *Am J Physiol - Gastrointest Liver Physiol* 286: 1032–1041, 2004. doi: 10.1152/AJPGI.00473.2003/ASSET/IMAGES/LARGE/ZH30060416821008.JPEG.
40. **Kleme ML**, **Sané A**, **Garofalo C**, **Seidman E**, **Brochiero E**, **Berthiaume Y**, **Levy E**. CFTR Deletion Confers Mitochondrial Dysfunction and Disrupts Lipid Homeostasis in Intestinal Epithelial Cells. *Nutr 2018, Vol 10, Page 836* 10: 836, 2018. doi: 10.3390/NU10070836.
41. **Shapiro BL**. Evidence for a mitochondrial lesion in cystic fibrosis. *Life Sci* 44: 1327–1334, 1989. doi: 10.1016/0024-3205(89)90389-5.
42. **Kelly-Aubert M**, **Trudel S**, **Fritsch J**, **Nguyen-Khoa T**, **Baudouin-Legros M**, **Moriceau S**, **Jeanson L**, **Djouadi F**, **Matar C**, **Conti M**, **Ollero M**, **Brouillard F**, **Edelman A**. GSH monoethyl ester rescues mitochondrial defects in cystic fibrosis models. *Hum Mol Genet* 20: 2745–2759, 2011. doi: 10.1093/HMG/DDR173.
43. **Lai N**, **Kummitha C**, **Drumm M**, **Hoppel C**. Alterations of skeletal muscle bioenergetics in a mouse with F508del mutation leading to a cystic fibrosis-like condition. *Am J Physiol - Endocrinol Metab* 317: E327–E336, 2019. doi: 10.1152/AJPENDO.00064.2019/ASSET/IMAGES/LARGE/ZH10081981320005.JPEG.
44. **Tam RY**, **van Dorst JM**, **McKay I**, **Coffey M**, **Ooi CY**. Intestinal Inflammation and Alterations in the Gut Microbiota in Cystic Fibrosis: A Review of the Current Evidence, Pathophysiology and Future Directions. *J Clin Med* 11: 649, 2022. doi: 10.3390/JCM11030649.
45. **Than BLN**, **Linnekamp JF**, **Starr TK**, **Largaespada DA**, **Rod A**, **Zhang Y**, **Bruner V**, **Abrahante J**, **Schumann A**, **Luczak T**, **Niemczyk A**, **O'Sullivan MG**, **Medema JP**, **Fijneman RJA**, **Meijer GA**, **Van Den Broek E**, **Hodges CA**, **Scott PM**, **Vermeulen L**, **Cormier RT**. CFTR is a tumor suppressor gene in murine and human intestinal cancer. *Oncogene 2016 3532* 35: 4191–4199, 2016. doi: 10.1038/onc.2015.483.
46. **Strubberg AM**, **Liu J**, **Walker NM**, **Stefanski CD**, **MacLeod RJ**, **Magness ST**, **Clarke LL**. Cftr Modulates Wnt/β-Catenin Signaling and Stem Cell Proliferation in Murine Intestine. *Cell Mol Gastroenterol Hepatol* 5: 253–271, 2018. doi: 10.1016/J.JCMGH.2017.11.013.

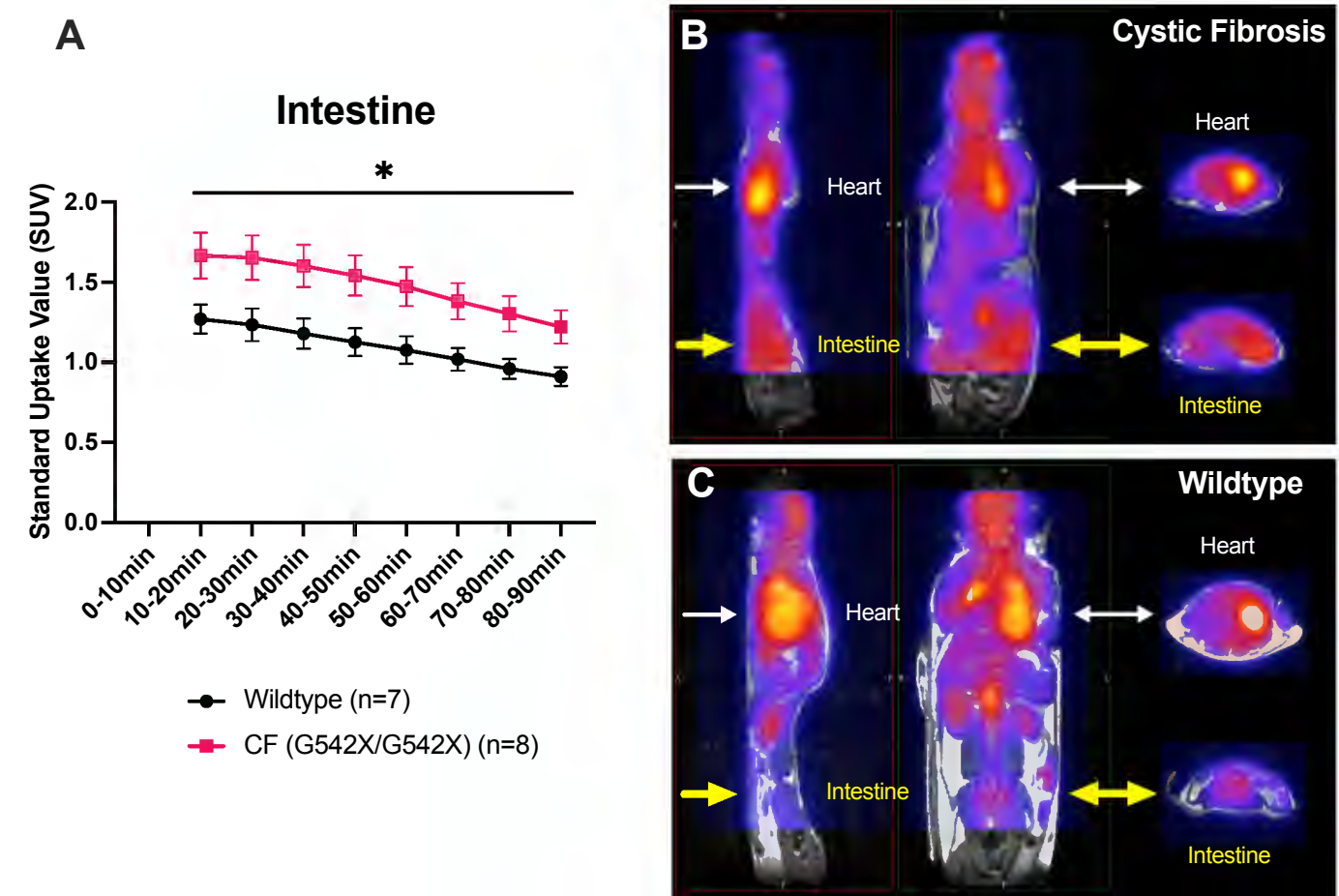
A
Intestine
*
Standard Uptake Value (SUV)
2.0
1.5
1.0
0.5
0.0
0-10min
10-20min
20-30min
30-40min
40-50min
50-60min
60-70min
70-80min
80-90min
Wildtype (n=7)
CF (G542X/G542X) (n=8)
B
Cystic Fibrosis
Heart
Intestine
Heart
Intestine
C
Wildtype
Heart
Intestine
Heart
Intestine

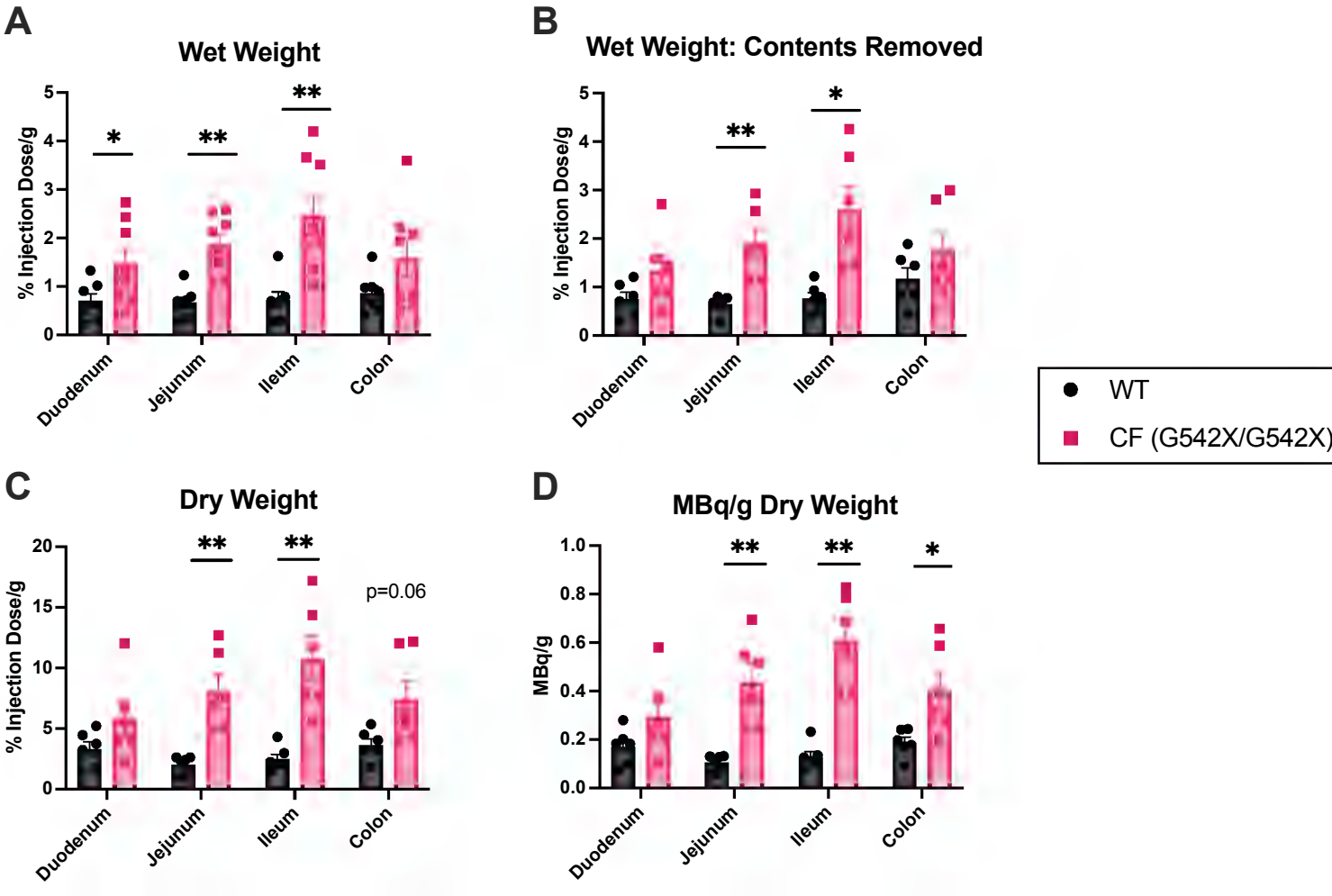
A
Wet Weight
% Injection Dose/g
0
1
2
3
4
5
*
**
**
Duodenum
Jejunum
Ileum
Colon
B
Wet Weight: Contents Removed
% Injection Dose/g
0
1
2
3
4
5
**
*
Duodenum
Jejunum
Ileum
Colon
WT
CF (G542X/G542X)
C
Dry Weight
% Injection Dose/g
0
5
10
15
20
**
**
p=0.06
Duodenum
Jejunum
Ileum
Colon
D
MBq/g Dry Weight
MBq/g
0.0
0.2
0.4
0.6
0.8
1.0
**
**
*
Duodenum
Jejunum
Ileum
Colon

A

Glucose Transporter Gene Expression - Signficance (RNASeq)

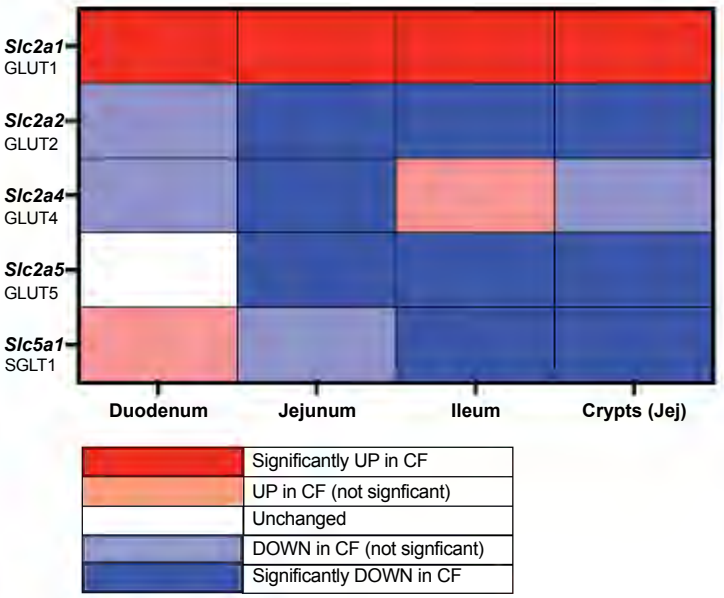

	Significantly UP in CF
	UP in CF (not signficant)
	Unchanged
	DOWN in CF (not signficant)
	Significantly DOWN in CF

B

Glucose Transporter Gene Expression - Log2 Fold Change (RNAseq)

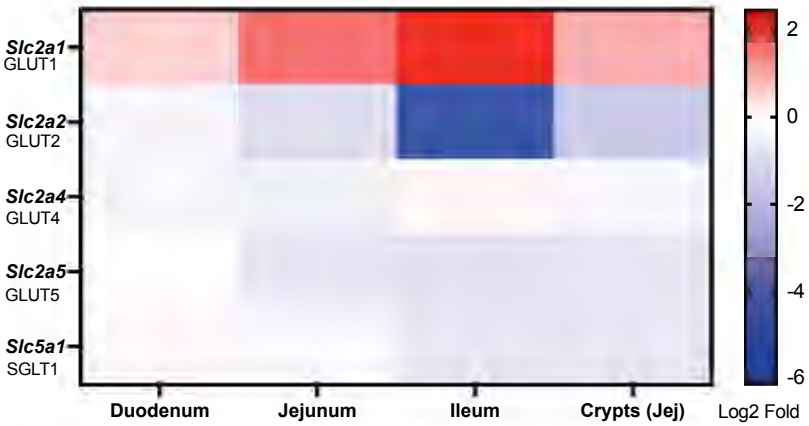

C

Wildtype Mouse **Small Intestine** - (Single Cell RNA Seq)

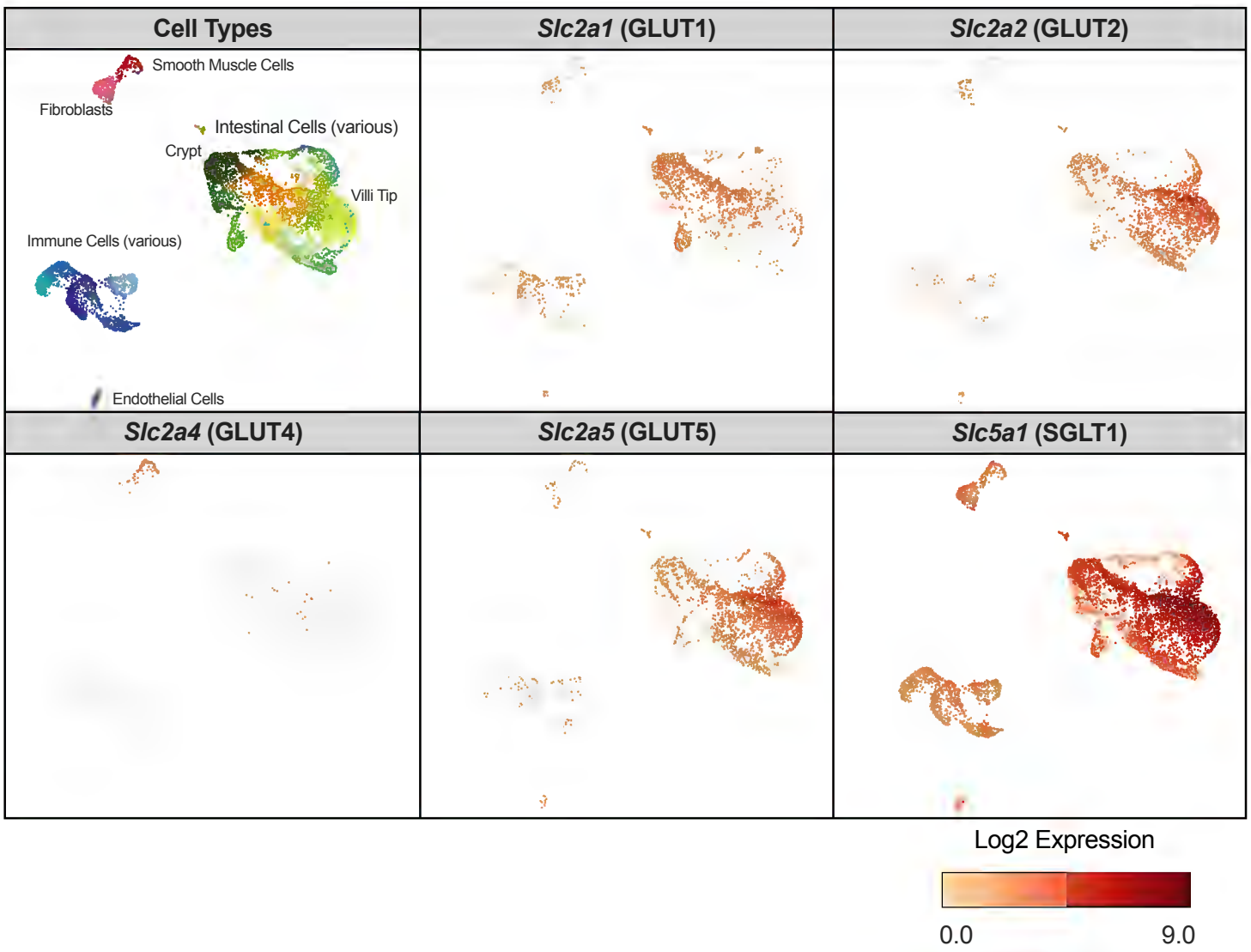

A

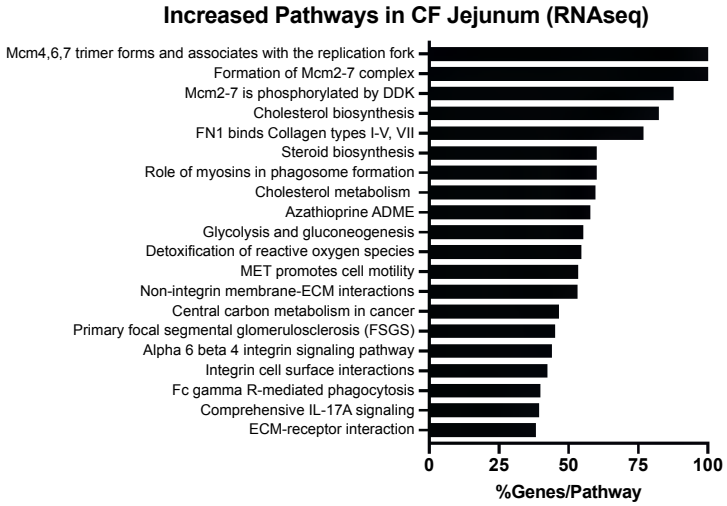

B

Adjusted p-value (Pathway)	Glycolysis/ Gluconeogenesis (KEGG)	Glycolysis and Gluconeogenesis (WP)	Glycolytic process (GO BP)
Duodenum	ns	ns	ns
Jejunum	4.92E-07	1.04E-05	7.51E-06
Ileum	9.84E-05	9.64E-06	6.96E-04
Crypts (Jejunum)	2.20E-06	6.83E-06	5.86E-06

C

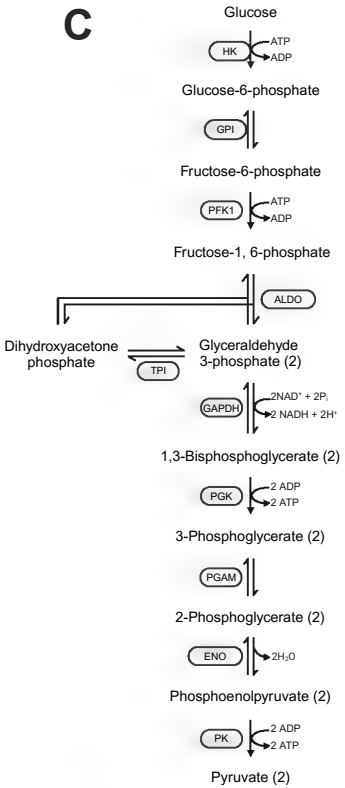

D

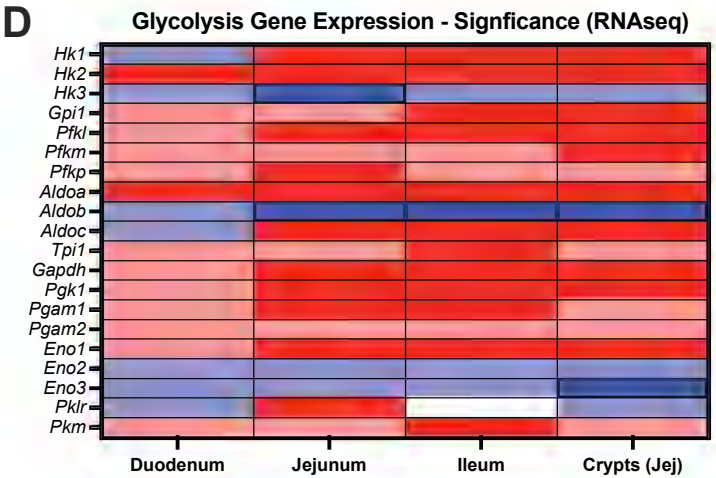

	Significantly UP in CF
	UP in CF (not signficant)
	Unchanged
	DOWN in CF (not signficant)
	Significantly DOWN in CF

E

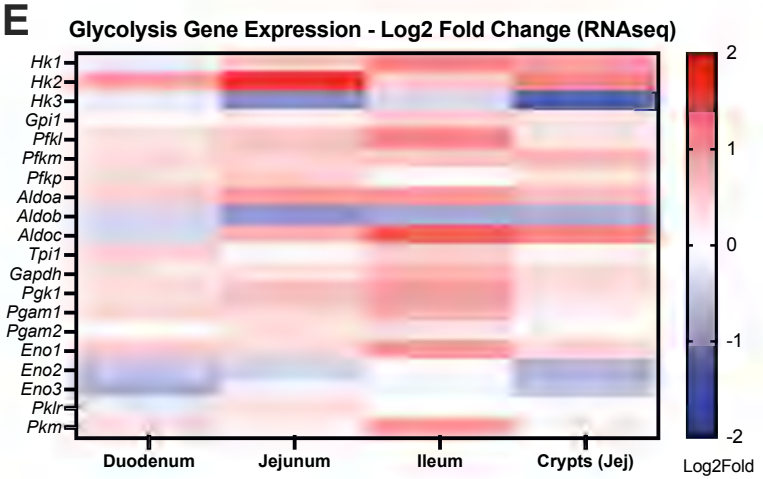

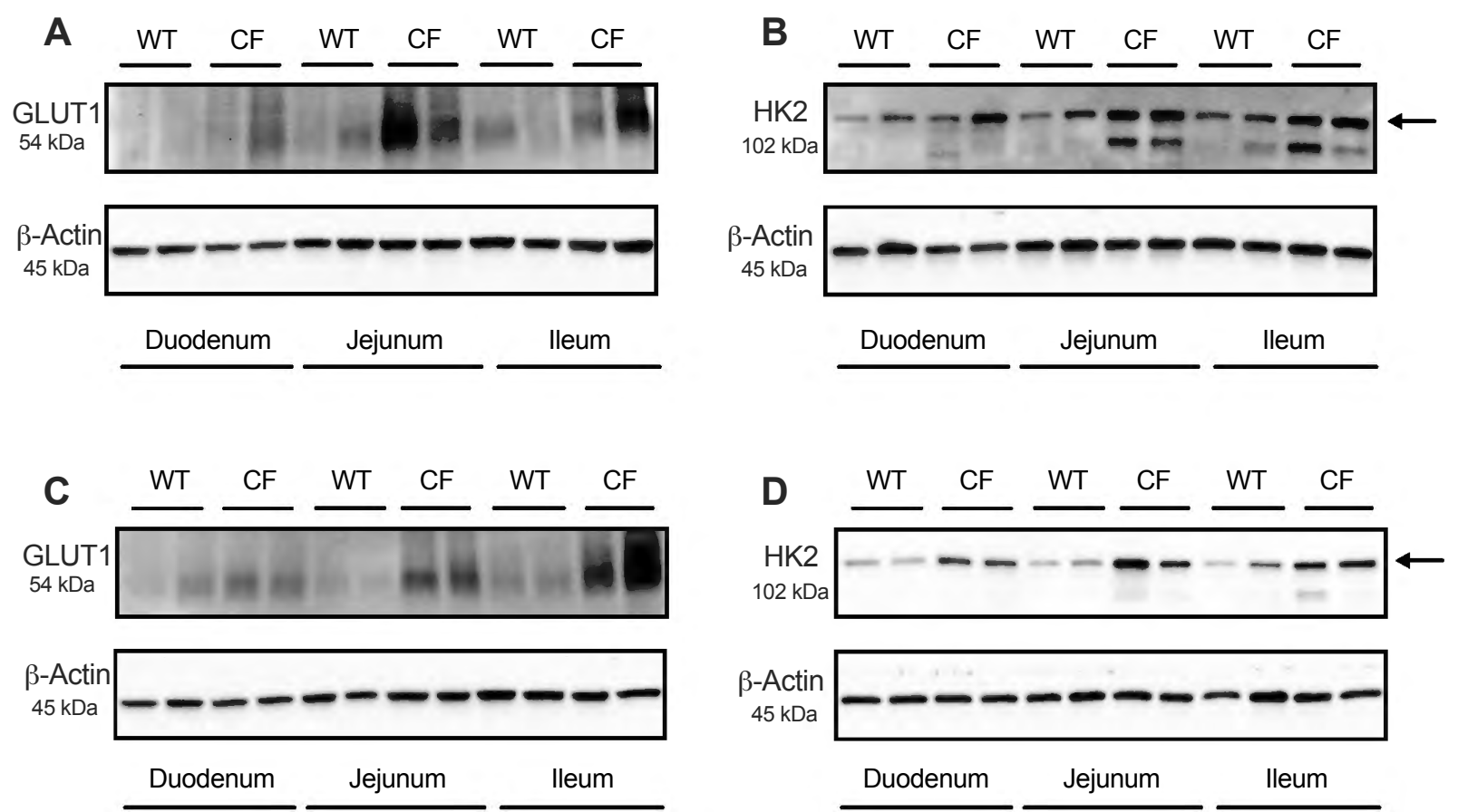
A
WT
CF
WT
CF
WT
CF
GLUT1
54 kDa
β-Actin
45 kDa
Duodenum
Jejunum
Ileum
B
WT
CF
WT
CF
WT
CF
HK2
102 kDa
β-Actin
45 kDa
Duodenum
Jejunum
Ileum
C
WT
CF
WT
CF
WT
CF
GLUT1
54 kDa
β-Actin
45 kDa
Duodenum
Jejunum
Ileum
D
WT
CF
WT
CF
WT
CF
HK2
102 kDa
β-Actin
45 kDa
Duodenum
Jejunum
Ileum

Duodenum

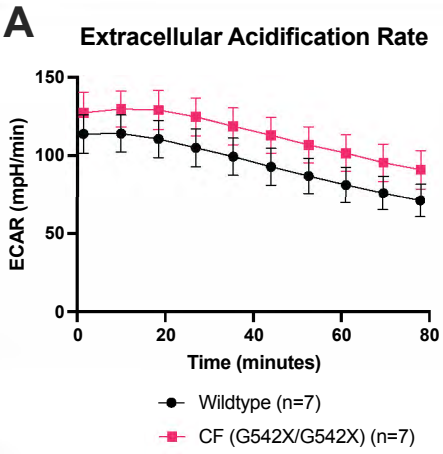

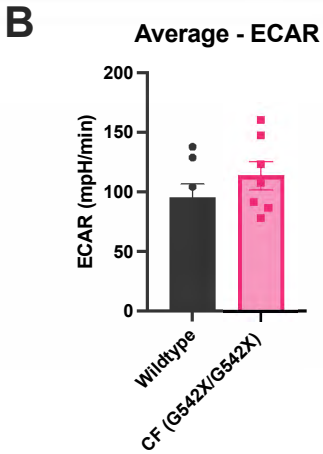

Jejunum

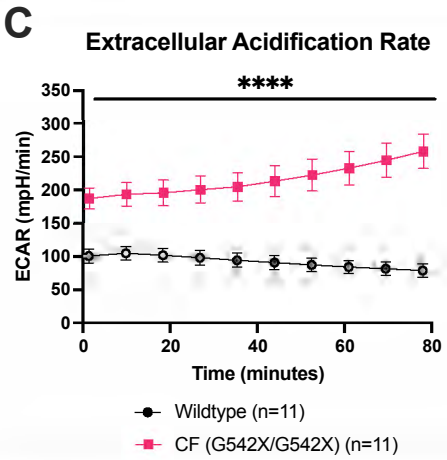

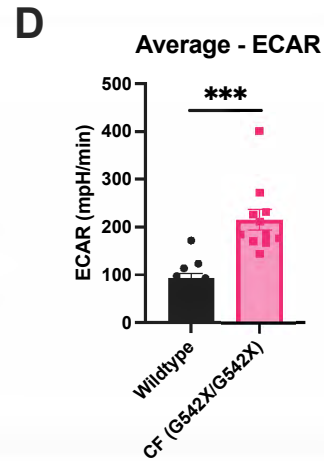

Ileum

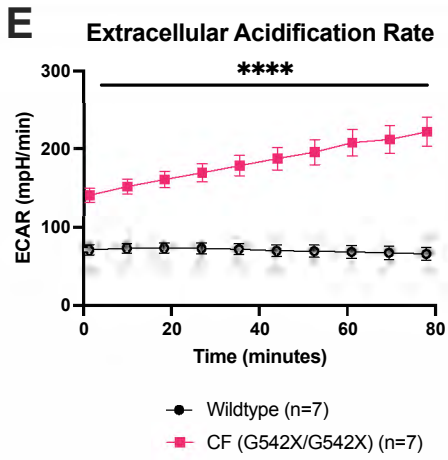

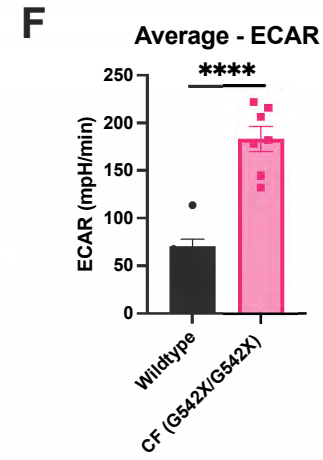

Lactate

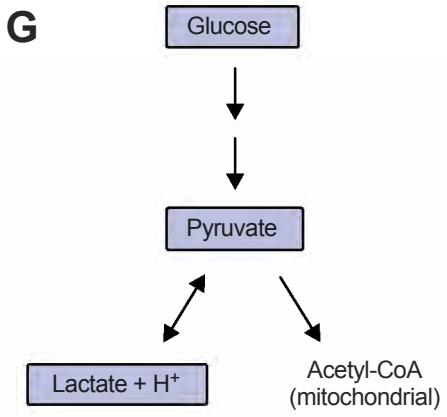

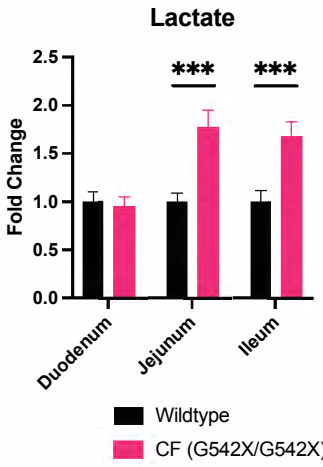

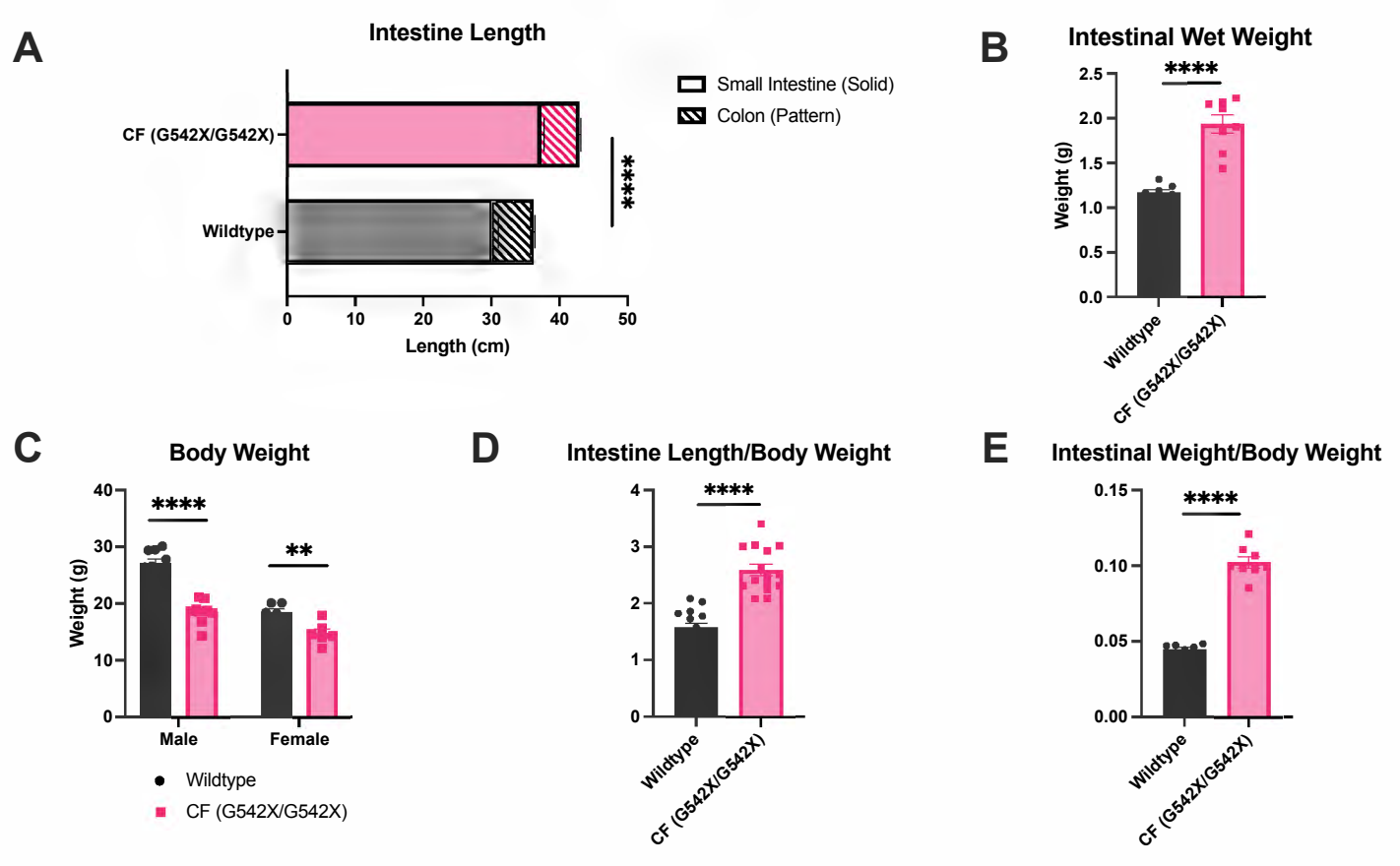
A
Intestine Length
Small Intestine (Solid)
Colon (Pattern)
CF (G542X/G542X)
Wildtype
****
0
10
20
30
40
50
Length (cm)
B
Intestinal Wet Weight
****
Weight (g)
2.5
2.0
1.5
1.0
0.5
0.0
Wildtype
CF (G542X/G542X)
C
Body Weight
****
**
Weight (g)
40
30
20
10
0
Male
Female
Wildtype
CF (G542X/G542X)
D
Intestine Length/Body Weight
****
4
3
2
1
0
Wildtype
CF (G542X/G542X)
E
Intestinal Weight/Body Weight
****
0.15
0.10
0.05
0.00
Wildtype
CF (G542X/G542X)

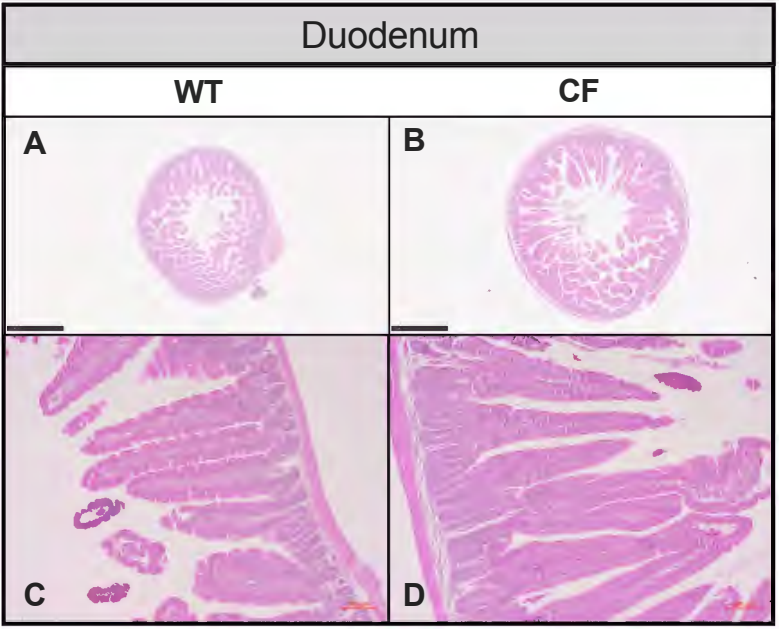

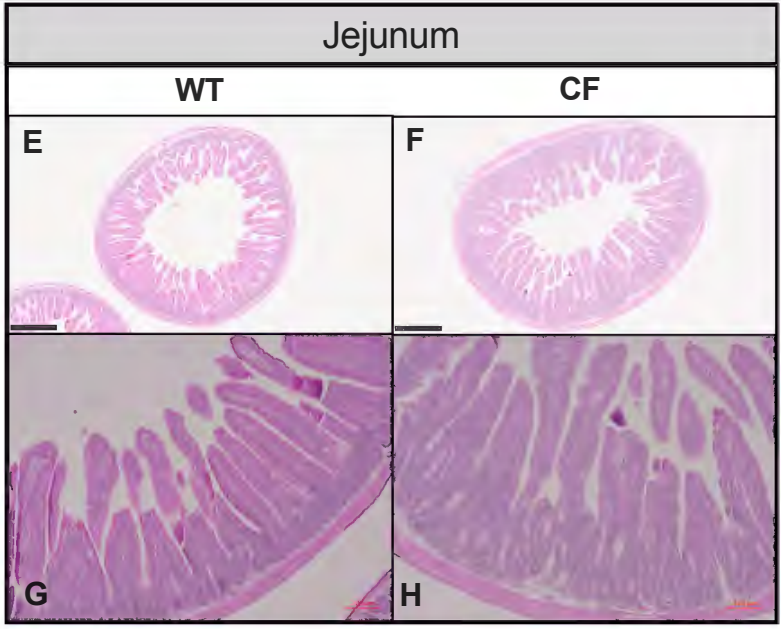

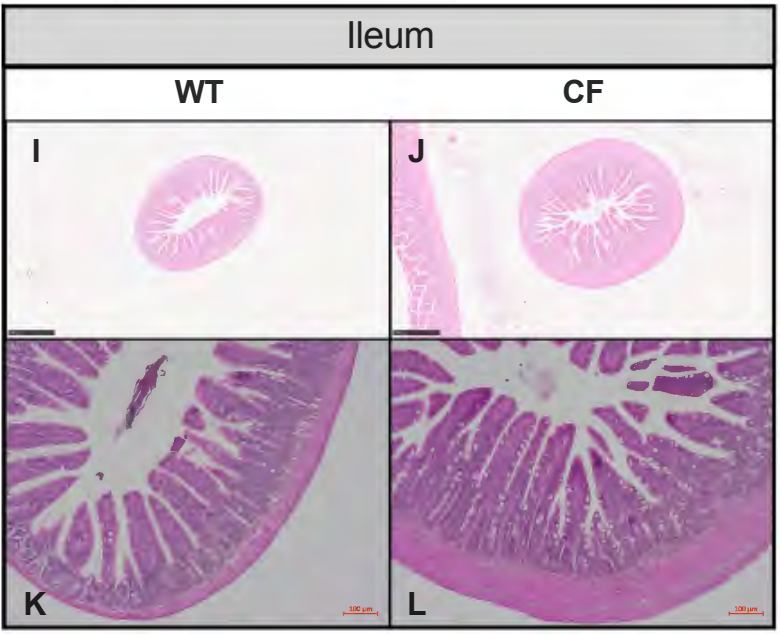

M

	Genotype	Villi (µm)	Crypts (µm)	Crypt + Villi (µm)	Smooth Muscle (µm)
Duodenum	WT	289 ± 12.2	73 ± 1.3	361 ± 12.4	30 ± 1.4
	CF	379 ± 10.6 ***	116 ± 2.4 ***	495 ± 11.1 ***	40 ± 1.4 ***
Jejunum	WT	194 ± 7.5	72 ± 1.4	265 ± 8.1	32 ± 1
	CF	245 ± 5.5 ***	145 ± 2.4***	390 ± 6.5 ***	65 ± 2 ***
Ileum	WT	135 ± 4.2	68 ± 1.6	204 ± 5	47 ± 2
	CF	187 ± 3.8 ***	136 ± 2.8 ***	322 ± 5.1 ***	129 ± 4.2 ***

N

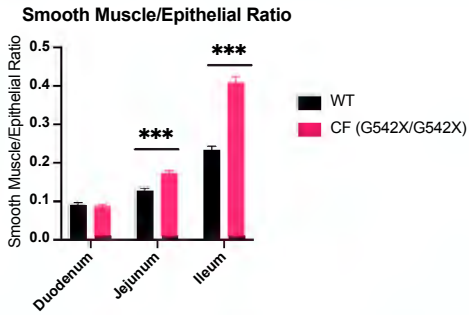

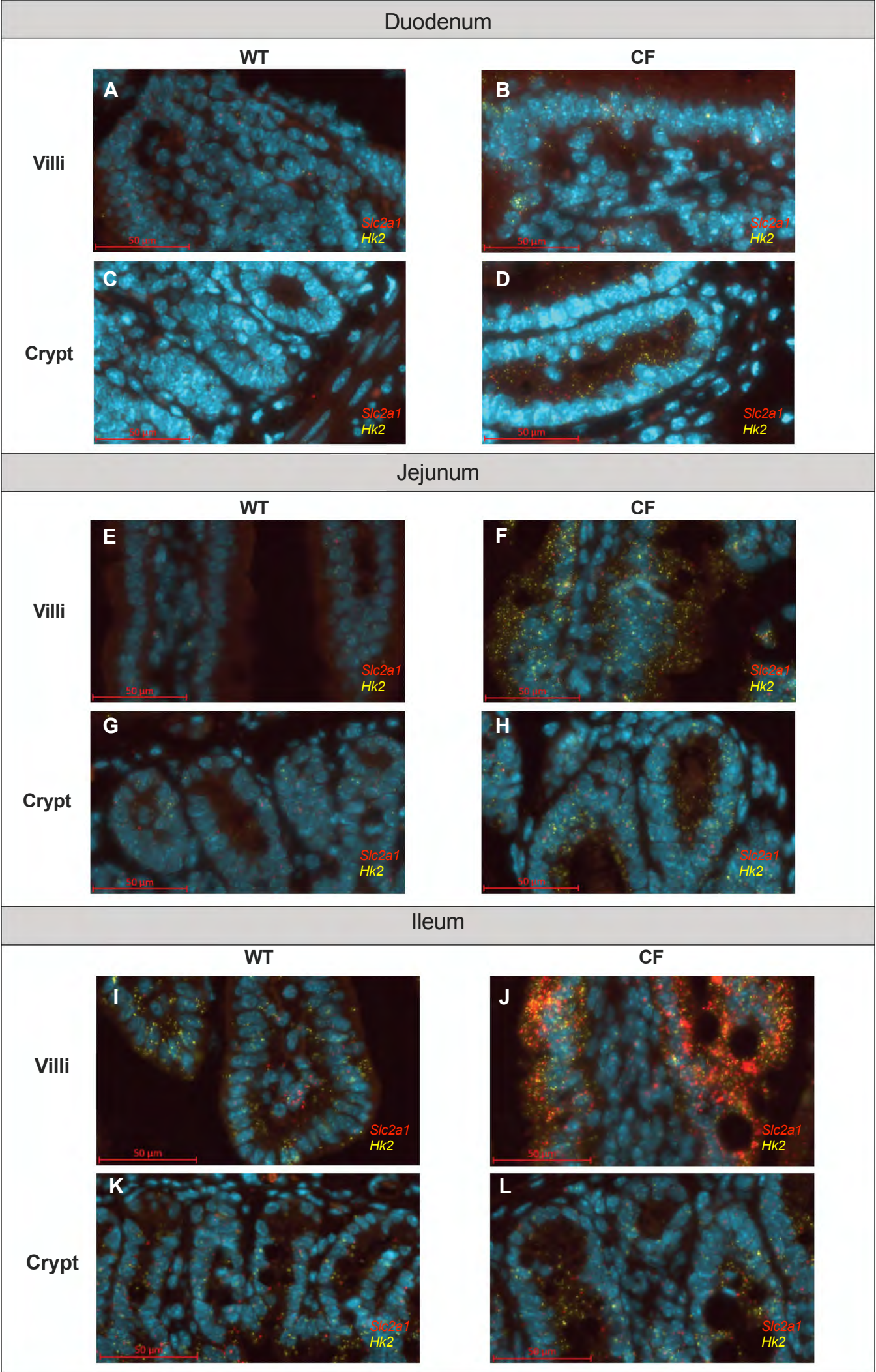
Duodenum
WT
CF
Villi
Crypt
A
B
C
D
Jejunum
E
F
G
H
Ileum
I
J
K
L
Slc2a1
Hk2
50 µm

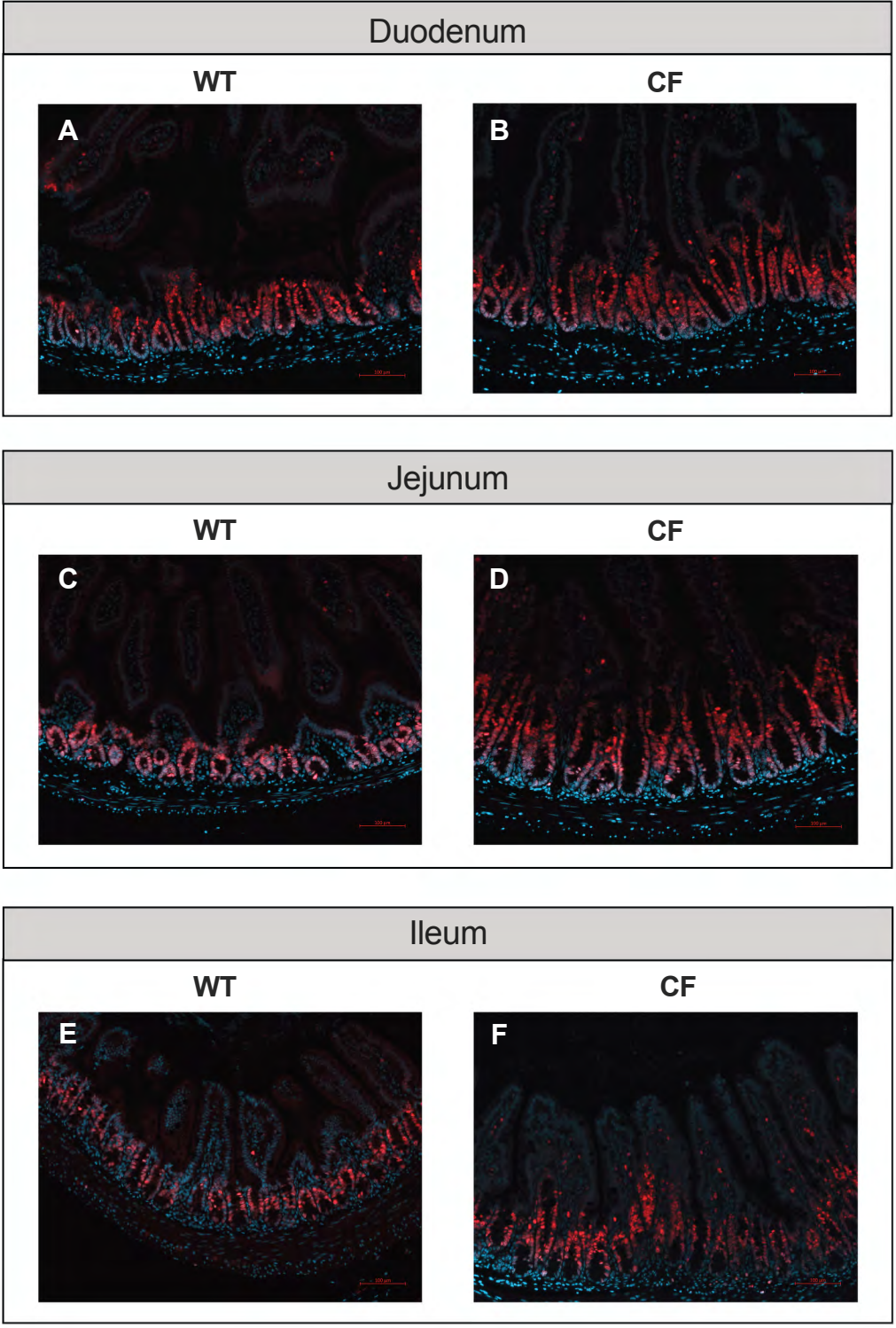
Duodenum
WT
CF
A
B
Jejunum
WT
CF
C
D
Ileum
WT
CF
E
F

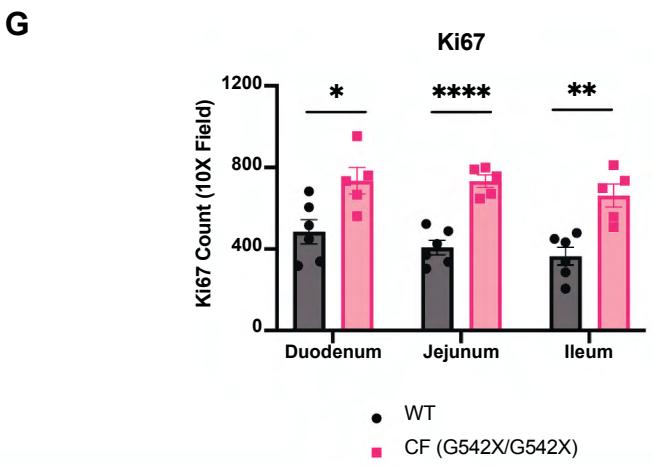
G
Ki67
Ki67 Count (10X Field)
1200
800
400
0
*
****
**
Duodenum
Jejunum
Ileum
WT
CF (G542X/G542X)

Wildtype

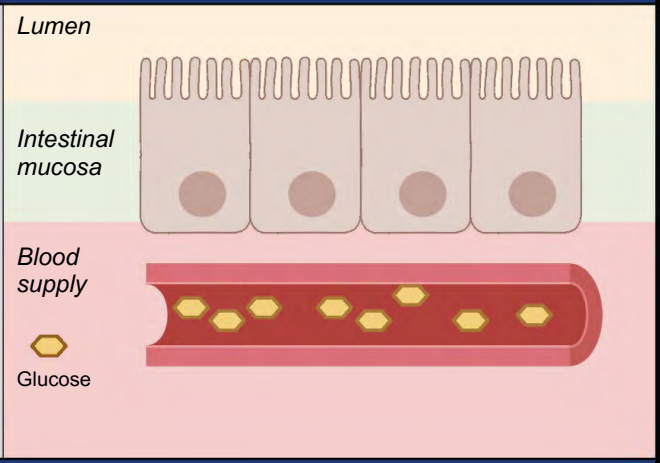

Cystic Fibrosis

Intestinal adaptations → Increased intestinal glucose demand